Summer 2021

# Structural Studies of the von Willebrand Factor D' domain and its Binding Mechanism to Factor VIII

AP Wang
*Western Washington University*, ap.wangp@gmail.com

# *Structural Studies of the von Willebrand Factor D' domain and its Binding Mechanism to Factor VIII*

By

AP Wang

Accepted in Partial Completion
of the Requirements for the Degree
Master of Science

ADVISORY COMMITTEE

Dr. P. Clint Spiegel Chair

Dr. Jeanine Amacher

Dr. Sergey Smirnov

GRADUATE SCHOOL

David L. Patrick, Dean

**Master's Thesis**

In presenting this thesis in partial fulfillment of the requirements for a master's degree at Western Washington University, I grant to Western Washington University the non-exclusive royalty-free right to archive, reproduce, distribute, and display the thesis in any and all forms, including electronic format, via any digital library mechanisms maintained by WWU.

I represent and warrant this is my original work, and does not infringe or violate any rights of others. I warrant that I have obtained written permissions from the owner of any third party copyrighted material included in these files.

I acknowledge that I retain ownership rights to the copyright of this work, including but not limited to the right to use all or part of this work in future works, such as articles or books.

Library users are granted permission for individual, research and non-commercial reproduction of this work for educational purposes only. Any further digital posting of this document requires specific permission from the author.

Any copying or publication of this thesis for commercial purposes, or for financial gain, is not allowed without my written permission.

AP Wang

August 18th, 2021

# *Structural Studies of the von Willebrand Factor D' domain and its Binding Mechanism to Factor VIII*

A Thesis
Presented to
The Faculty of
Western Washington University

In Partial Fulfillment
Of the Requirements for the Degree
Master of Science

by
AP Wang
August 2021

## Abstract

Hemophilia A is an X-linked disorder that results in uncontrolled bleeding, which is caused by a lack of activity for blood coagulation factor VIII, an essential protein cofactor in the clotting cascade. Factor VIII consists of multiple domains, and binding disruptions between factor VIII and its circulatory partner, von Willebrand Factor, may cause von Willebrand disease. Von Willebrand Disease type 2N is an autosomal recessive disease, and it is caused by binding disruptions between the D' domain (also known as TIL'E') of von Willebrand Factor and a3 domain of factor VIII. A 2.9Å Cryoelectron microscopy structure of the FVIII:vWF complex was recently published, and this crystal structure further described the interactions between FVIII and vWF. To further understand the most severe types of von Willebrand Disease type 2N, site-directed mutagenesis of vWF was employed to enhance the understanding of binding disruptions between vWF and FVIII. The designed mutants were transformed, expressed, and purified for further experimental studies. Binding assays were conducted between the mutants against our bioengineered chimeric structure factor VIII, ET3i, via pull-down assays, sedimentation assays, as well as quantitative studies via biolayer interferometry. The results of this present study included the investigation of binding studies between the D' domain of von Willebrand factor and the a3 domain of factor VIII. The results obtained in this study were interpreted, compared, and concluded to be consistent with the newest cryo-EM structure.

**Acknowledgements**

The work conducted in this study was undertaken in the Spiegel lab at Western Washington University from Fall of 2019 to Summer of 2021. I wish to first and foremost thank Dr. P. Clint Spiegel for accepting me into his research group and the opportunity that he's given me to work on this project, as well as his time, and guidance throughout the duration of my study. I also wish to offer my sincerest gratitude to Dr. Kenneth. C. Childers for his time, patience, kindness, and leadership that he has provided and exemplified in the Spiegel Lab. I would like to also acknowledgement previous graduate students who worked on various aspects of the blood project, specifically Michelle E. Wuerth and Joey Gish, who have paved the way for my study here. Lastly, I wish to thank my cohort; Shaun Peters, Micah Nakao, Haley Wofford, and Erin Rosenkranz, for their unwavering support these past two years.

The D' plasmid and sequence were provided by Dr. Flemming Hansen at the University of College London. The ET3i construct was provided by Expression Therapeutics, LLC and I would like to thank Dr. Christopher Doering and Dr. Gabriela Denning for providing an abundance in the ET3i construct for all research conducted within the blood project. I wish to offer my gratitude to my thesis committee, Dr. P. Clint Spiegel, Dr. Jeanine Amacher, and Dr. Serge Smirnov for their assistance and commentary on the final drafts of this manuscript. My thanks to all faculty to Western Washington University, for supporting and understanding all students during the pandemic.

Finally, my utmost thanks to Marie Lenac for her patience, sacrifice, and continued support (with more tears than sweat and blood) during my graduate studies.

# Table of Contents

## Abbreviations

Ab- Antibody

AMC- Anti-Mouse IgG $F_c$ capture

Amp- Ampicillin

BLI- biolayer interferometry

BME- β-mercaptoethanol

CV- column volume

Cryo-EM- cryo-electron microscopy

EM- electron microscopy

ET3i- (bioengineered chimeric structure, fVIII)

DOPC- dioleoyl phosphatidylcholine

DOPS- dioleoyl phosphatidylserine

$F_{AB}$- antigen binding fragment

$F_C$- constant fragment

GP- glycoprotein

HBS- HEPES buffered saline

HEPES- 2-[4-(2-hydroxyethyl)piperazin-1-yl]ethanesulfonic acid

IgG- immunoglobin G

IMAC- Immobilized metal affinity chromatography

IPTG- Isopropyl β-D-1-thiogalactopyranoside

ITI- Immune tolerance therapy

LB- Luria-Bertani

MW- molecular weight

NEB- New England Biosciences

NTA- nitrilotriacetic acid

OD- optical density

PEG- polyethylene glycol

PMSF- phenylmethanesulfonylfluoride

PS- Phosphatidylserine

RPM- rotations per minute

SDS- sodium dodecyl sulfate

SDS-PAGE- sodium dodecyl sulfate-polyacrylamide gel electrophoresis

SEC- size exclusion chromatography

TEV- tobacco etch virus

TIL- trypsin-inhibitor-like

Tris- 2-amino-2-hydroxymethyl-1,3-propanediol

Tris-HCl- 2-amino-2-hydroxymethyl-1,3-propanediol-hydrochloride

TRX- thioredoxin

vWD- von Willebrand Disease

vWF- von Willebrand Factor

v/v- volume by volume

w/v- weight by volume

# List of Figures and Tables

# Introduction

The layout of this thesis will be presented in five Chapters. Chapter one discusses the overall physiological context of this research project. First, it will detail the blood coagulation cascade in the traditional cascade as well as the improved cell-based model. This will include the intrinsic pathway, extrinsic pathway, along with how disruptions of these pathways may cause hemophilia. The primary hemophilia of interest, hemophilia A, along with von Willebrand Disease will be presented. Lastly, the therapeutic treatments for these diseases will be presented.

Chapter two details the project's protein of interest: first, factor VIII and von Willebrand Factor (vWF) along with previous structural findings. Second, domains of von Willebrand factor will be discussed, specifically, the D' (TIL'E') region. The binding mechanism and dissociation from activated factor VIII of the D' domain will be reviewed. Lastly, an anti-factor VIII antibody will be introduced in this chapter, and their respective significance to factor VIII will be described in the following chapters.

Chapter three describes the specific regions of factor VIII, C1, C2, and the A3 domain. Structural studies will be presented along with their significance to the protein of interest; D' domain of vWF. Next, mutations in vWF will be introduced along with the reason why these mutants were chosen for study.

Chapter four details the progress towards the D' domain of von Willebrand Factor along with the mutants of this selected domain. Progress achieved in the lab include transformation, protein expression via *E.coli* bacterial expression system, chromatographic purification methods, as well as SDS-PAGE verification method. Additionally, binding studies will be detailed

between constructs of factor VIII and vWF. Lastly, the utilization of X-ray crystallography and how it was applied in this study.

Chapter five tackles the results obtained via a series of various binding assays along with X-ray crystallography. This final chapter will also detail the reaffirmation and discussion of the current binding mechanism between vWF and factor VIII.

# Chapter 1

## Introduction to Blood Coagulation

Upon vascular injury, there is a two-phased response termed "hemostasis" that is initiated to prevent excessive blood loss and to preserve vital blood supply in the body. The first phase is primary hemostasis, where the body initiates reduction of blood flow to the trauma site. Platelets then aggregate at the vessel near the trauma site and form a "soft-plug"; this involves platelet adhesion and platelet aggregation.[1] This platelet rich "soft-plug" provides a surface for the assembly of coagulation proteins during secondary hemostasis, where the "soft-plug" is reinforced with a tough fibrin clot.

Secondary hemostasis deploys an activated thrombin in which it proteolytically attacks the fibrinogen to form fibrin. The cross-linked fibrin will then form a clot across the trauma site to prevent excessive bleeding.[1] In order for secondary hemostasis to occur, it relies on a "waterfall" event involving a network of proteins and a multitude of circulatory protein cofactors (factors I-XIII) to create localized coagulation to the site of injury. This is known as the blood coagulation cascade.[2]

The initially perceived single "waterfall" course, the blood coagulation cascade was described in two pathways with a shared destination: the *intrinsic* and *extrinsic* pathways that lead to the final *common pathway*.[2] The *common pathway* leads to thrombin promoted insoluble fibrin clot formation. The initially published description of the coagulation cascade was perceived as a sequential cascade of protein interactions without consideration of extracellular activity (Figure 1).[2] During blood vessel injury, the *extrinsic pathway* is initiated from the

exposed tissue factor (TF) protein that is expressed on the subendothelial cells that is extravascular. The tissue factor protein activates factor VII (FVIIa), and the TF:FVIIa in the presence of calcium activates factor X (FXa). The *intrinsic pathway* relies on activated Factor XII (FXIIa) creating activated Factor XI (FXIa), which then activates factor IX (FIXa). On the other hand, thrombin cleaves factor VIII (FVIII) which is circulating in the bloodstream in complex with its carrier protein, von Willebrand Factor (vWF) to yield activated factor VIII (FVIIIa). FVIIIa in complex with FIXa is known as the *intrinsic tenase complex*.[2] The tenase complex in the common pathway is composed of FXa:FVa which cleaves factor II (FII, also known as prothrombin) to yield activated factor II (FIIa, also known as thrombin). In turn, thrombin cleaves factor I (fibrinogen) into fibrin (FIa). Fibrin is cross-linked by activated factor XIII (FXIIIa) to form stable fibrin clots (Figure 1).[2]

Unfortunately, this "waterfall" or cascade model described has been noted to be insufficient in explaining the entire blood coagulation process, as the intrinsic and extrinsic pathway cannot function independently to form a stable blood clot. Therefore, an improved cell-based model is utilized to explain the coagulation cascade in detail. This model describes the cascade in three distinct but intersecting phases: initiation, amplification, and propagation.[3]

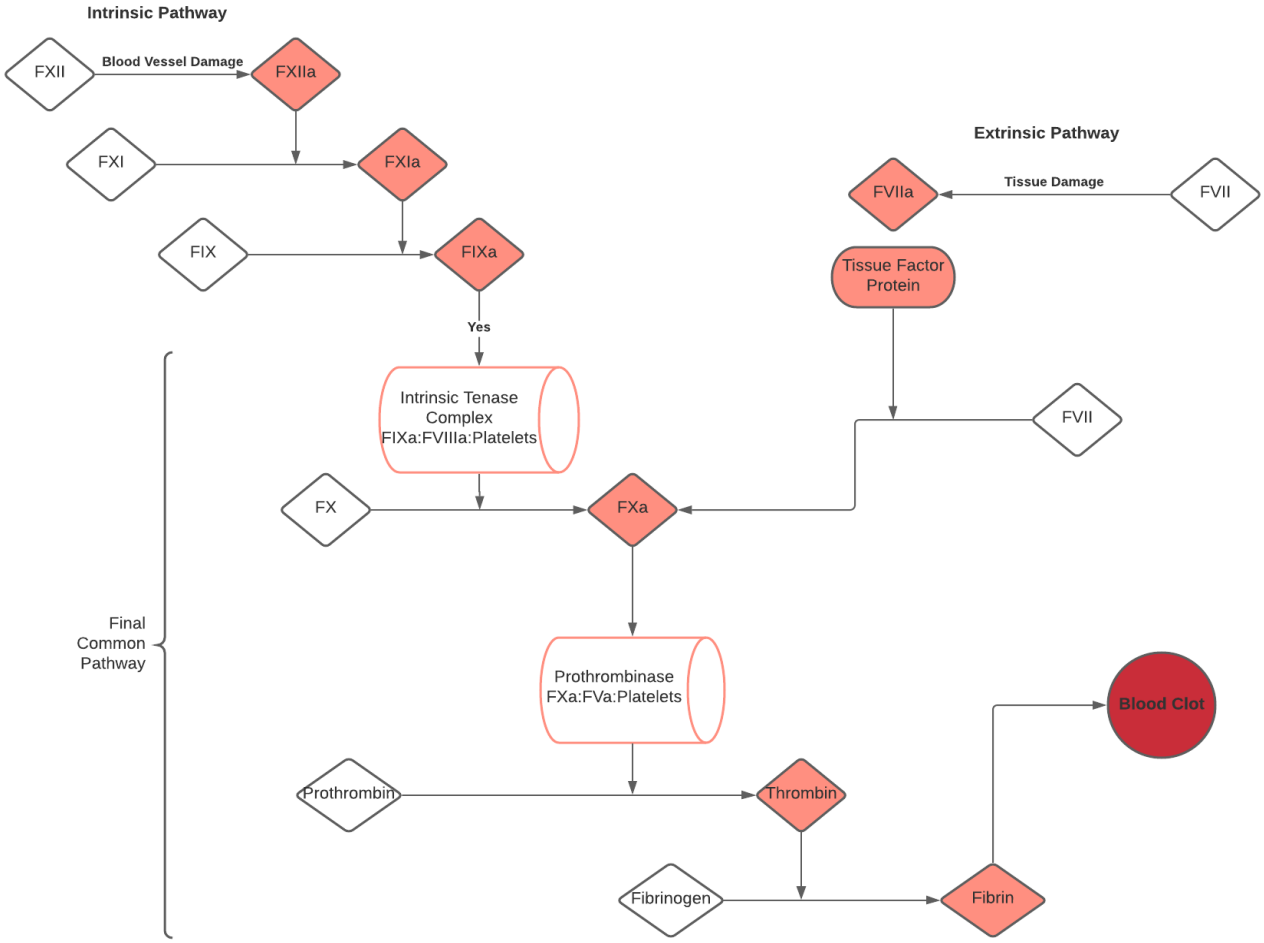


Figure 1. Flow schematic of the blood coagulation cascade (adapted from Davie and Ratnoff 1964).[2] The traditional coagulation cascade portrays the *intrinsic pathway* and *extrinsic pathway* converging to the *final common pathway*. The *intrinsic pathway* is initiated upon blood vessel injury, which activates FVII. FXIIa then activates FXI to form the *intrinsic tenase complex* (FXIIa:FXIa). The *extrinsic pathway* is stimulated by trauma, which activates FVII. The TF:FVIIa complex along with the *intrinsic tenase complex* together activate FX. This leads to the final *common pathway*, FXa forms the prothrombinase complex with FVa (FXa:FVa) in the presence of calcium to generate large amounts of thrombin (FII). Fibrin is then generated from fibrinogen to form a stable blood clot which is then deployed to the site of injury to control excessive blood loss.

**Phase one: Initiation**

*Initiation*- This is the first phase of hemostasis, traditionally known as the extrinsic pathway of the coagulation cascade. This phase is stimulated by tissue damage, which results in the expression of tissue factor protein on the surface of endothelial cells. Given this, the initiation step is localized on tissue factor-presenting cells (e.g. fibroblast cells), which are extravascular. Upon tissue damage, tissue factor along with circulatory proteases activate factor VII. FVII is then exposed to the bloodstream. Then, FVIIa associates itself with its transmembrane receptor, TF, forming the TF:FVIIa complex to activate factor IX in the presence of calcium (Figure 2). Additionally, tissue damage causes platelet adhesion to other extracellular components which increases the secretion of partially activated factor V.[3] The activation of factor V can also be achieved by thrombin, or activated factor X to form the *extrinsic tenase complex* (factor X:factor V). The *Tenase complex* serves to convert prothrombin into thrombin, which functions as the signal for platelet activation in this phase.

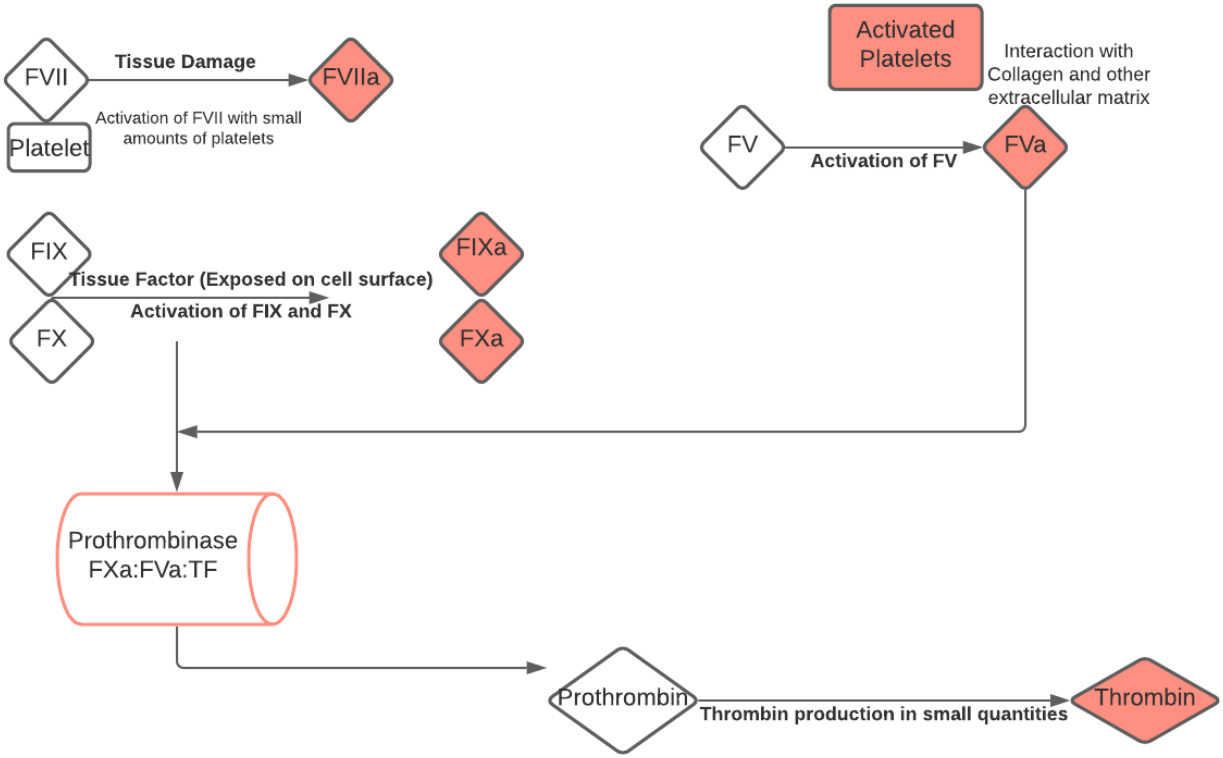


Figure 2. Flow schematic of phase one of secondary hemostasis: *initiation*, also traditionally known as the *extrinsic pathway* of the blood coagulation cascade (adapted from Davie and Ratnoff 1964).[2] In this phase, factor VII is activated via tissue damage. Tissue factor that's exposed on the cell surface binds to activated factor VII which then activates small amounts of factor IX and factor X. Simultaneously, activated platelets bind to collagen along with other extracellular matrixes to activate factor V. This leads to the factor X: factor V: tissue factor complex known as *prothrombinase*. This complex produces small amounts of thrombin for the next phase of hemostasis: amplification.

**Phase Two: Amplification**

*Amplification*- This is the second phase of hemostasis, which results in an increase level of activated coagulation factors (Figure 3). The thrombin produced during the initiation phase then activates factor V, factor VIII, and factor XI on platelet surfaces during this phase (resulting in

factor Va, factor VIIIa, and factor XIa). The amplification phase sets the stage for the upcoming large-scale production of thrombin in the propagation phase.[3]

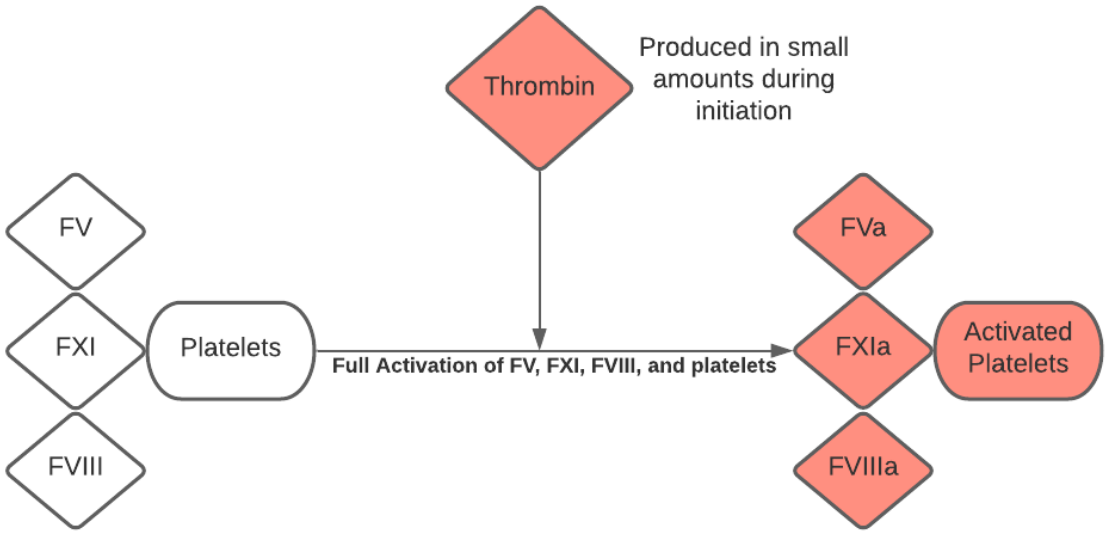


Figure 3. Schematic of Phase two of the secondary hemostasis: *Amplification* (adapted from Davie and Ratnoff 1964).[2] In this phase, the levels of FVa, FXIa, FVIIIa, and activated platelets are elevated from the small amounts of thrombin generated in the initiation phase. Elevated levels of these factors are utilized in the third phase, propagation.

**Phase Three: Propagation**

*Propagation*- This is the final phase of hemostasis, contrary to the initiation phase, this is traditionally known as the *intrinsic* pathway of the coagulation cascade. This phase is stimulated by blood vessel damage and takes place on the surface of the activated platelets. In this stage, a large influx of thrombin is produced to convert soluble fibrinogen into insoluble fibrin clots. In order to do so, FVIIa activates FXIa which in turns activates FIXa allowing formation of the

*intrinsic tenase complex* (FVIIIa:FIXa). The *intrinsic complex* then activates prothrombinase complex (FXa:FVa) generated in the initiation phase to produce an increased amount of thrombin to proteolytically convert soluble fibrinogen into insoluble fibrin. These insoluble fibrils are then gathered at the site of injury to form a stable, hard clot (Figure 4). The importance of the improved cell-based model is to explain hemostasis *in vivo*, where the extrinsic FVIIa:TF activated FX can't compensate for the missing FVIII/FIX activity in hemophiliacs.[3]

The complete hemostasis process is complex and involves multivariable components, and all components in secondary hemostasis play a crucial role in the success of a stable blood clot formation. Any discrepancies within the complete hemostasis would result in coagulation complication. However, the focus of this study will be on blood coagulation factor VIII. Factor VIII plays a central role in the formation of the *intrinsic tenase complex* in the propagation phase.

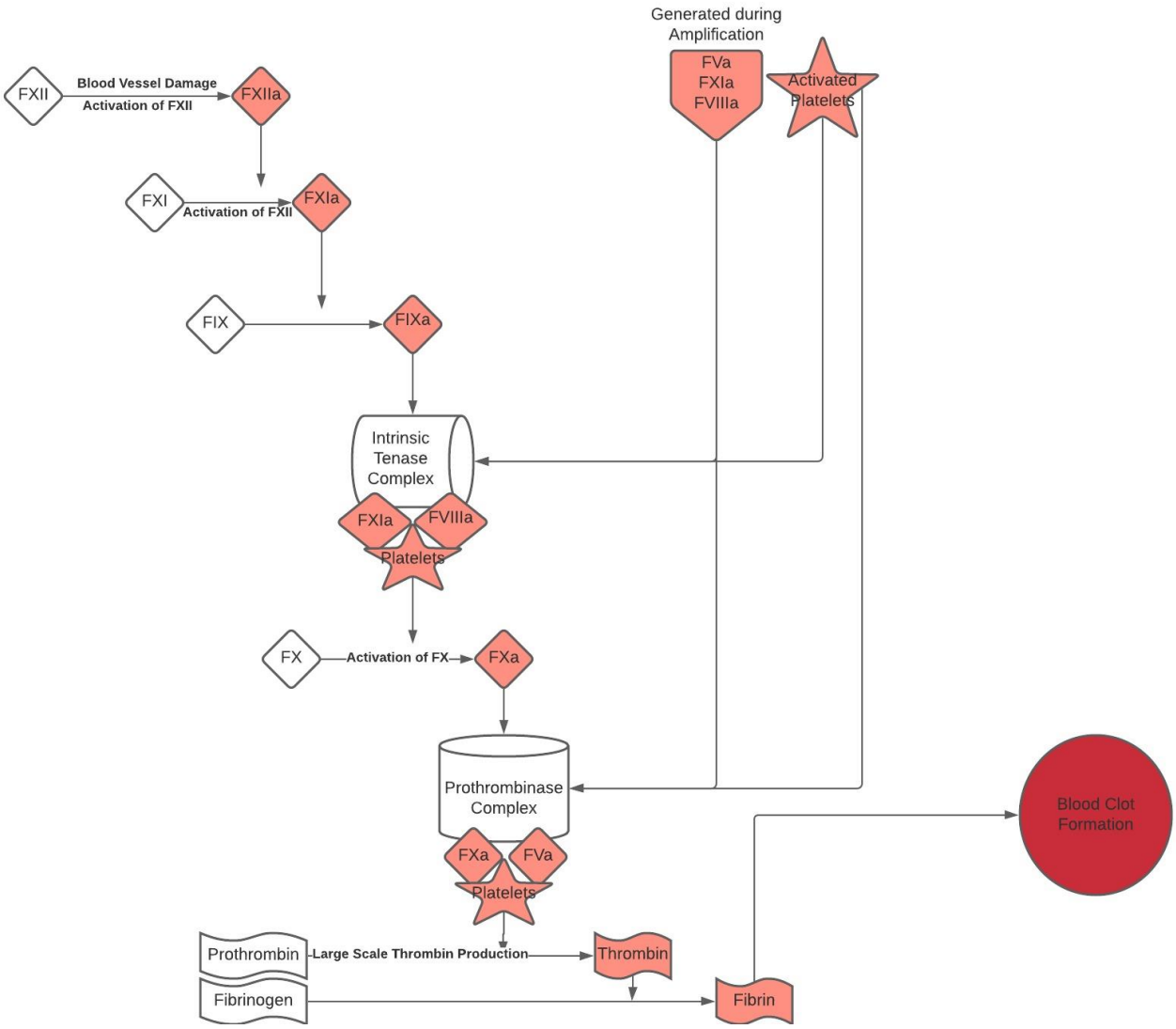


Figure 4. The final phase of secondary hemostasis: propagation (adapted from Davie and Ratnoff 1964).[2] This is also traditionally known as the intrinsic pathway of the blood coagulation cascade. Propagation is initiated by blood vessel damage, or, vascular damage which activates factor XII. Activated factor XII then activates factor IX which then forms the intrinsic tenase complex, composing of activated factor XI, factor VIII, and platelets. The tenase complex then activates factor X which is then utilized in forming the prothrombinase complex composing of activated factor X, factor V, and activates platelets. The prothrombinase complex then generates large scale thrombin production which then proteolytically converts soluble fibrinogen into insoluble fibrin. The insoluble fibrin then accumulates into long fibrils and gather at the trauma site to form a stable blood clot.

**Introduction to Blood Coagulation Factor VIII**

Factor VIII is a glycoprotein that plays a critical role in the formation of a stable and proper blood clot. FVIII is mostly synthesized in the hepatic sinusoidal cells.[4] Mature FVIII is initially synthesized as a multi-domain single polypeptide that consists of 2332 residues. Domains of FVIII upon expression are as follows: A1-a1-A2-a2-B-a3-A3-C1-C2.[5] The A domains include short spacers (a1, a2, and a3), containing acidic regions with groups of negatively charged amino acids: aspartic and glutamic acid. Additionally, the three A domains have been found to have sequence homology to one another. Similarly, the two C domains have significant homology to each other as well. Lastly, the B domain does not observe any homology to other proteins. Previous studies have also indicated that the absence of B domain does not affect FVIII functionality, and therefore undergoes proteolytic cleavage early in FVIII life cycle at residues Arg1313 and Arg1648.[5] This cleavage forms a noncovalent heterodimer consisting two sectors: the *heavy chain* (A1-A2-B) and *light chain* (A3-C1-C2) (Figure5).[5]

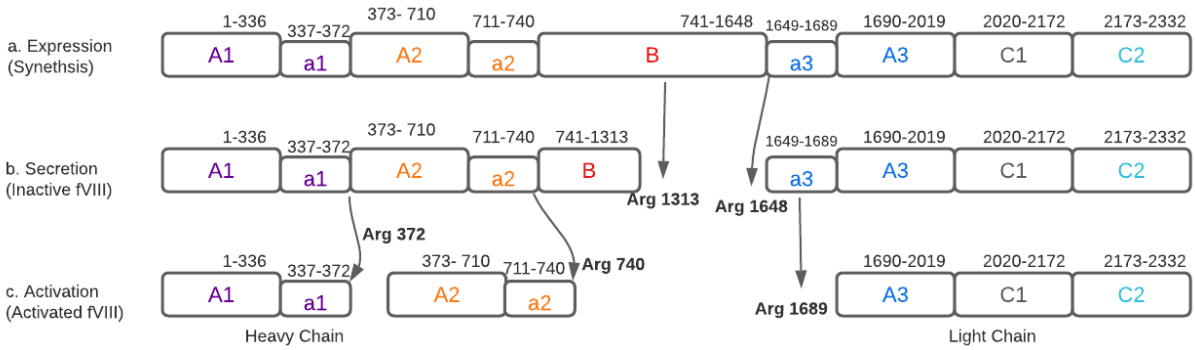


Figure 5. Schematic review of the construct of FVIII (adapated from Kauffman, 1988).[6] FVIII is initially synthesized in a single polypeptide consisting of 2332 residues (A1-a1-A2-a2-B-a3-A3-C1-C2). The lower-case domains (a1, a2, and a3) are acidic linker regions to their respective domains. FVIII cleavage occurs at residues Arg1313 and Arg1648 resulting in secretion out of the cell as an inactive heterodimer. (A1-a1-A2-a2-B/ a3-A3-C1-C2). FVIII is then activated by thrombin cleavage at Arg372, Arg740, and Arg1689.

FVIII circulates the bloodstream in its inactive form, noncovalently bound to its circulatory partner, von Willebrand Factor. This interaction between the two glycoprotein prevents the premature dissociation of FVIII in circulation as it is not stable if not in complex with vWF. Additionally, this interaction is also thought to prevent premature binding of FVIII to FIXa along with activated platelet surfaces.[7,8]

Previous studies show that two specific regions of the FVIII light chain is involved in vWF binding: the acidic region of the A3 domain (residues 1649-1689) as well as the carboxy terminus of the C2 domain (Figure 6).[9] FVIII is only proteolytically activated into a heterodimer upon activation. FVIIIa then dissociates from its circulatory partner, vWF, along with removal of the acidic a3 region of FVIII.[8–10] FVIIIa then binds to the activated platelet surfaces, and in the presence of calcium ions, serves as a cofactor for serine protease FIXa. This complex is also known as the *intrinsic tenase complex* and is responsible for large scale activation of FX.

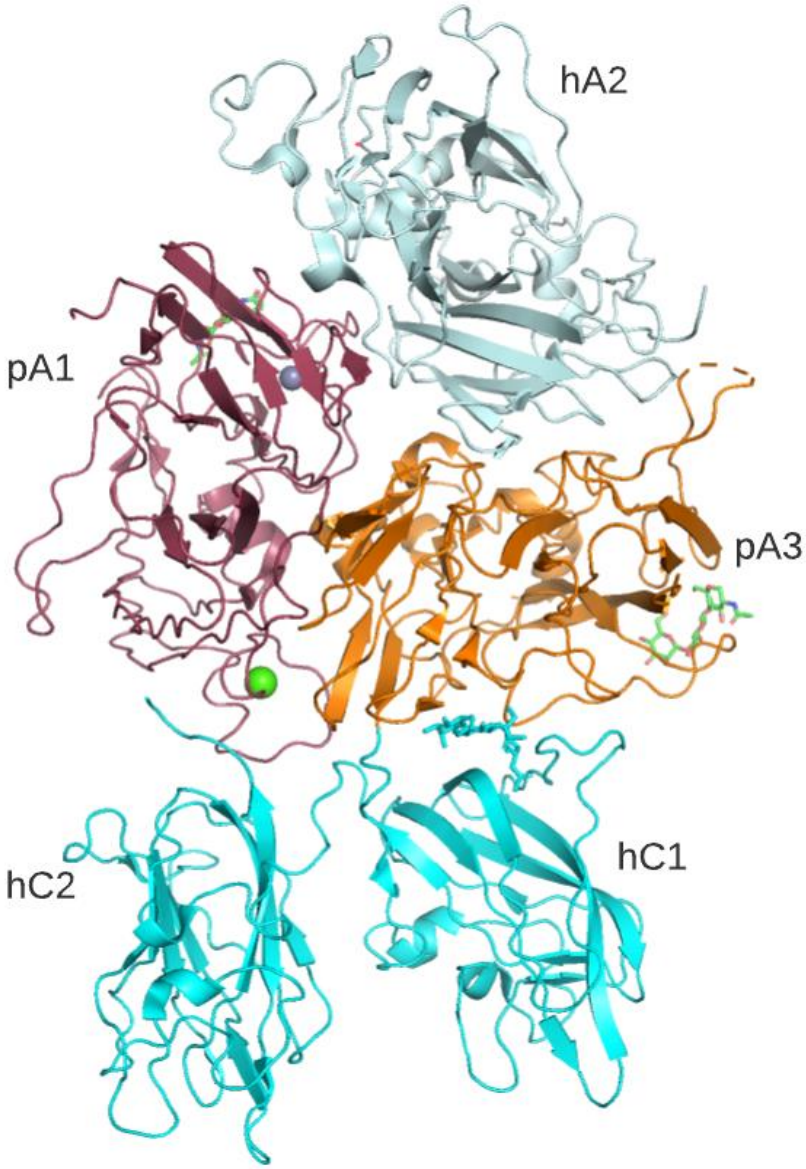


Figure 6. X-Ray Crystal Structure of bioengineered chimeric FVIII, ET3i. This is a B domain deleted FVIII heterodimer composed of heavy chain (porcineA1- humanA2) and light chain (porcine A3-C1-C2). C1 observes similar homology with C2, and the C domains have been proposed to be involved in vWF binding (PDB ID 6MF2).[11]

## Hemophilia A

Hemophilia is a disorder that affects the body's ability to maintain homeostasis by forming stable blood clots. There are many forms of hemophilia. Briefly, the cause of hemophilia A is the decreased activity of FVIII, the cause of hemophilia B is the deficiency of functionality of FVIII, and the cause of hemophilia C is the deficiency of Factor XI (FXI) and parahemophilia which is a deficiency of Factor V (FV). In this study, hemophilia A is the primary disease of interest for discussion.

There are four DNA mutations that may take place, leading to hemophilia A: deletions, insertions, inversions, and substitution. Each of these mutations may affect function, structural integrity, or both. More specifically, protein sequence mutations can be classified as null, truncation, or point. A null mutation results in complete loss of protein expression, or complete absence of the protein of interest that is encoded by the gene. A truncation mutation may result in only partial expression of target protein. Finally, a point mutation (substation) is where a specific amino acid at a specific location change to another; this can have a significant impact on protein function as well as structure. Mutations that take place in the binding domains of FVIII to vWF may result in hemophilia A, specifically point mutations.

Hemophilia A is a blood clotting disorder that is caused by the lack of activity for the protein cofactor (FVIII). Hemophilia A is a X-linked blood disorder that prevents proper blood clot formation, and this disorder affects approximately one in every 5000 males.[12] Hemophilia A is characterized by excessive or prolonged bleeding episodes where a blood clot is unable to properly form at the site of injury. The severity of this disorder is dependent on the degree of dysfunctional FVIII present. Mild hemophilia A is defined with approximately 6-30% normal

FVIII activity, moderate is categorized as 1-5% normal FVIII functionality, and severe with less than 1% normal activity.[13] The 186 kb gene coding of the FVIII protein (F8) is located on the long arm of the X-chromosome, position 28.[14] There are many different possible mutations within the F8 gene that can heavily affect protein activity during coagulation. Acquired hemophilia is another form of hemophilia that does not involve a genetic mutation basis. Acquired hemophilia occurs when the body produces antibodies against FVIII which results in rapid dissociation from its circulatory partner vWF and loss of function.

**Hemophilia A Therapeutic Treatments**

Replacement therapy is currently the most widely used method for Hemophilia A in the United States. Replacement therapy consists of infusion of either direct plasma derived or recombinant human FVIII (hFVIII) concentrates.[15] These infusions can be utilized as episodic infusions or as prophylactic treatments for severe hemophilia A. Episodic infusions refer to replacement of hFVIII after each bleeding episode, to replenish FVIII and thereby stabilize the bleeding episode. Prophylactic treatment on the other hand, refers to regular infusions (often two to three times a week) of FVIII concentrates as hemorrhagic prevention, i.e., reduction in the number of bleeding episodes and thereby improving the patient's quality of life. The disadvantage is that the patient will be required to visit their physician to receive these infusions two to three times per week, which is a demanding schedule. These replacements aren't always mutually exclusive, i.e., on top of prophylactic replacement therapy, on-demand (plasma derived) treatment is often utilized in emergency situations.

Plasma derived hFVIII was first discovered and heavily utilized as the primary method for hemophilia A treatment. In this method, FVIII is prepared by extracting along with purification of the glycoprotein from cryoprecipitate prepared from human plasma.[16] There are complications associated with this method upon its initial discovery, and that is transmission of viral containments and diseases. However, with improving technology and enhanced testing, transmission of viral contamination has been eradicated. Additionally, technology has been developed to advance disease detection prior to utilization of replacement therapy.[17] Recombinant FVIII are primarily produced by Chinese Hamster Ovary (CHO) cells or Baby Hamster Kidney (BHK) cells transfected with hFVIII gene.[18] To ensure safety prior to infusion, the concentrated proteins are subjected to viral inactivation methods.

Various recombinant FVIII products are available in the states; common recombinant FVIII therapeutics include Xyntha by Pfizer, Advate by Baxter, and Kogenate FS by Bayer Pharm. Doses of each of these products is based on the patient's level of FVIII deficiency, weight, and amount of bleeding. These products are usually injected intravenously via IV bolus upon a bleeding episode to encourage proper homeostasis. In 2015, Adynovate (BAX 855), a PEGlyated full length recombinant hFVIII based on Advate, was approved for both episodic and prophylactic treatment.[19] Adynovate has an extened half-life due to the addition of polyethlene glycol on the recombinant hfVIII, and thus serving as a better therapeutic for hemophilia A.

**Hemophilia A Treatment Complications**

Even with the high efficacy of these infusions, approximately 30% of the patients who receive direct transfusion of hFVIII eventually develop inhibitory antibodies, an immune response leading to the clearance of FVIII from circulation. This inhibitory response leaves the patient with difficulty maintaining homeostasis due to hFVIII being cleared from circulation. Although Immune responses have been noted with patients with mild to severe hemophilia A, it has been noted that patients with higher quantities of genetic mutations that lead to productions of non-endogenous FVIII often suffer from severe immune response. This is likely due to the patient's body not being able to recognize the FVIII as native.[20]

Immune tolerance induction (ITI) is a one treatment utilize to combat the inhibitory response by eradicating inhibitors that have been developed by the body and normalizing pharmacokinetic parameters. This is done by frequent administration of large doses of hFVIII, over long-term to eventually abolish the immune response against recombinant hFVIII. Immunosuppressive drugs or proteins are often accommodated in this treatment to ensure success and effectiveness. Due to the high levels of hFVIII often required to induce an immune tolerance, the treatment option is often extremely costly for patients; and can be physically taxing on patients with poor venous access. In addition to the potential financial challenges this treatment option poses, it is not successful in approximately 25% of cases. This leads to the ongoing need for additional alternative treatment options for hemophiliacs that suffer from extensive inhibitory responses.

To combat the anti-FVIII inhibitory response in patients, bypassing agents such as activated *prothrombin complex concentrates* (PCC, also known as the factor IX complex) and

recombinant activated factor VII replacements are utilized as primary therapies.[21] Porcine FVIII (pFVIII) is also often utilized as a treatment plan secondary to bypassing agents due to its low cross-reactivity to anti-FVIII antibodies. Another reason for pFVIII is considered a worthy substitute for FVIII replacement is that pFVIII more stable and more active than FVIII due to its A2 domain being in a tighter complex within its active form.

One of the main complications of replacement therapy in hemophilia is the formation of inhibitors neutralizing FVIII antibodies. This is due to the inhibitors rendering replacement treatment essentially ineffective due the half of life recombinant FVIII (rFVIII), and the body therefore concludes elimination of the recombinant protein as top priority. There have been strategies employed to produce less immunogenic hFVIII that maintains a longer half-life in circulation. Protein engineering has made this possible in the form of PEGylation. Addition of polyethylene glycol polymers to the targeted proteins have been shown to increase circulation time by masking the molecule that its attached to from the immune system and reducing clearance by the kidneys.[22] One of the recombinant hFVIII mentioned earlier, Adynovate, is a PEGylated form of recombinant hFVIII which provides it with an extended half-life to serve as a therapeutic. Furthermore, a recombinant factor VIII-Fc fusion protein (rFVIIIFc) has been constructed to potentially reduce the frequency of FVIII dosing with its extended half-life. RFVIIIFc is a recombinant fusion protein composed of recombinant FVIII and covalently bound to the Fc domain of immunoglobulin F1 Fc region (IgG1). Studies have shown that the Fc region of IgG1 has the potential to interact with immune cells expressing Fc receptor and thereby affecting the immune response to rFVIII.[23–25]

Lastly, bispecific antibody studies have also been utilized as therapeutic treatment for hemophiliacs. A bispecific monoclonal antibody is usually an artificial protein that combines two

or more antigen-recognizing elements into one construct, allowing it to simultaneously bind to two different antigens. A recent bispecific antibody, Emicizumad (ACE910), also known in the United States as HEMLIBRA®, has proven to be successful in Phase I clinical trials and well tolerated by healthy subjects. Emicizumad is noted to bind, and bridge activated factor IX and factor X, thereby acting as a factor VIII-mimetic agent.[26–28] Due to its unique structure, Emicizumab has not been subjected to recognition by FVIII inhibitors. More importantly, Emicizumab has a much longer half-life (approximately 4-5 weeks in healthy subjects) than recombinant FVIII. The bispecific antibody and its FVIII mimetic effects may abate both the frequent clinical visits and emergency visits for hemophiliacs.[28]

**FVIII and Inhibitory Antibodies: G99**

Detailed knowledge of the structural interactions between FVIII and its inhibitory antibodies are necessary to enhance and improve hemophilia A therapeutics; therefore, a thorough understanding of immunoglobulin G (IgG) is vital. Immunoglobulins contain a heavy chain and a light chain, which are identical to each other. In this Y-shaped monoclonal antibody ($M_{AB}$), there are two types of fragments: the constant fragment ($F_c$), and the antigen binding fragment ($F_{AB}$). As the name suggests, the $F_{AB}$s are responsible for binding to the antibody's target whereas the $F_c$ region of the antibody is conserved. Each antibody contains two $F_{AB}$s and they are located at the tips of the antibody's arm (Figure 7).

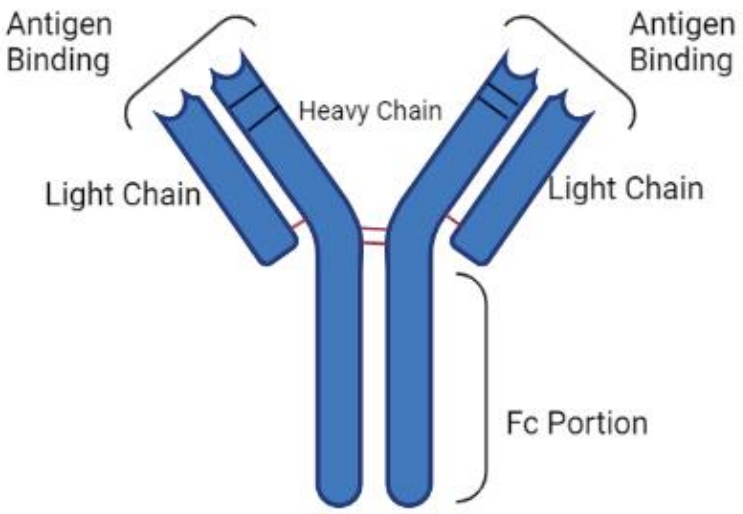


Figure 7. Schematic of antibody structure, the antibody consists of two separate $F_{AB}$. Light chain is noted to have the shorter arm, heavy chain noted on the inner (longer) arm of the "Y" shape, complementarity determining regions (CDRs) noted in black dash lines within the antigen binding site, and each of the $F_{AB}$s heavy and light chain are connected via disulfide bonds noted in red dashes.

Due to $F_{AB}$s high variability, it is able to bind to its target (antigen) with exceptional specificity. Each $F_{AB}$ contains two variable domains, one from the light chain and the other from the heavy chain. Within each of these variable domains, it contains three complementarity determining regions; and these contain variable loops that are responsible for recognizing specific regions of the antigens known as epitopes. This is the reason why $F_{AB}$s can bind to its antigen with such high specificity. The two $F_{AB}$s can be proteolytically cleaved from the $F_c$ domain via proteolytic enzyme papain (derived from papayas), allowing studies for antibody to antigen interactions by utilizing individual $F_{AB}$s bound to their protein of interest.

Characterization of immune responses on FVIII has shown that a large majority of antibodies against FVIII bind specifically to the A2 or C2 domains.[29] There are two categories of

antibodies that inhibit FVIII function: the classical antibody and the non-classical antibody. Classical antibodies are antibodies that directly block the binding of C2 domain to von Willebrand Factor or to phospholipid surfaces.[30] On the contrary, non-classical antibodies prevent FVIII activation by thrombin or FXa. For this research aim, only the nonclassical monoclonal antibody ($M_{AB}$) G99 was utilized for experimentation. Instead of the isolated C2 domain of FVIII, the chimeric structure of FVIII (ET3i) was utilized for this study which will be discussed later. Structural studies have shown that the epitope face where G99 $F_{AB}$ binds contains an electrostatic interaction where G99 has a negatively charged pocket that allowed the basic Lys2227 residue in the C2 domain to bind (Figure 8).[31]

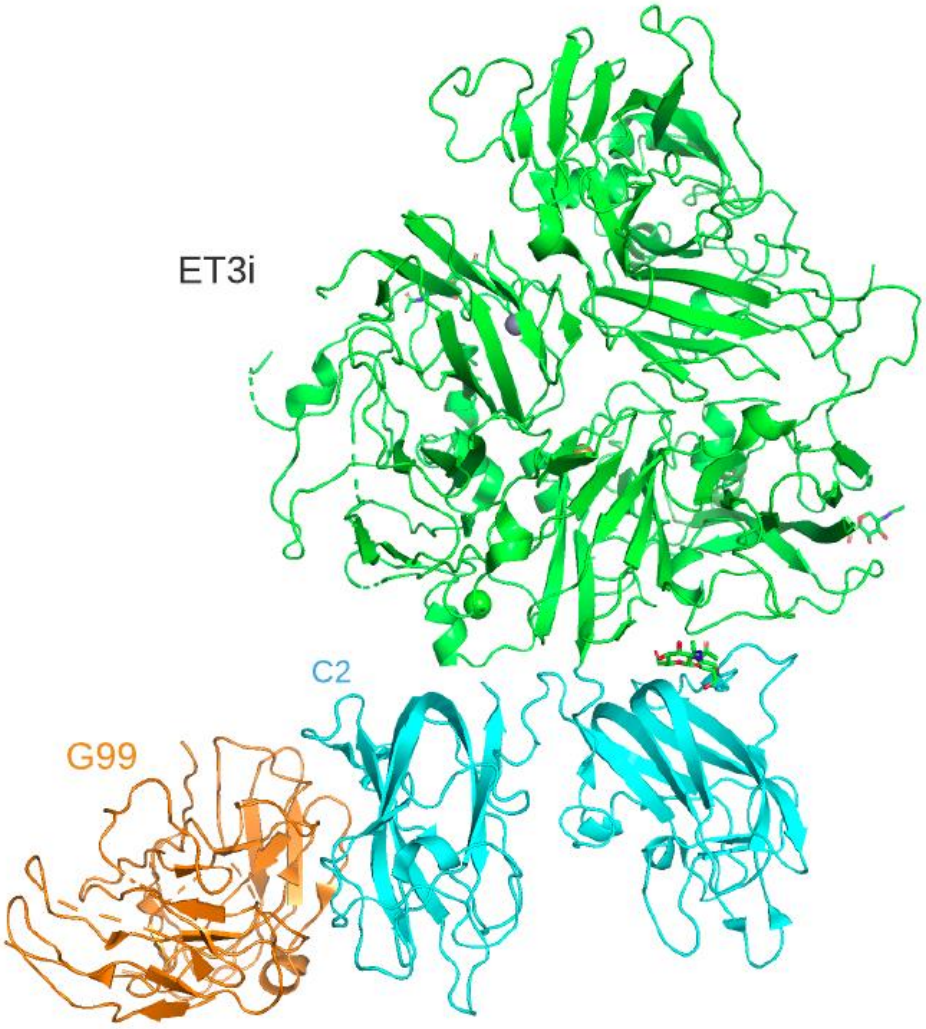


Figure 8. X-ray crystal structure of the chimeric FVIII structure, ET3i bound to a non-classical anti-C2 domain inhibitory antibody, G99 $F_{AB}$. C1 and C2 share structural homology, the C domains are noted in cyan. G99 $F_{AB}$ is depicted in green, bound to C2 at its basic pocket Lys2227. (PDB ID: 7KBT. Adapted from Ronayne et al. 2021).[32]

Chapter 2

## Introduction to von Willebrand Disease

As discussed in chapter 1, there has been substantial characterization of FVIII and its inhibitory antibodies. This has significantly enhanced our understanding of hemophilia A and its therapeutic treatments. However, there is an important interaction that is still not well known; FVIII and its circulatory partner, von Willebrand Factor (vWF) up until recently; even though it is one of the most inherited bleeding disorders in the world.[30] A recent high-resolution cryoeletron microscopy crystal structure of FVIII:D'D3 complex was published. This 2.9Å structure verified the important structural integrity and binding mechanism of D'D3 to FVIII. Structural knowledge of the FVIII:D'D3 will be introduced later in this chapter.

Von Willebrand disease was first discovered in the 1920's by a Finnish physician named Erik von Willebrand, from whom the disease was named. Von Willebrand first characterized this disease by studying a young girl's case whose family had extensive hemorrhagic difficulties.[33] The young girl's family was in the Finland's Åland islands during the study. With the island's smaller population, there is a higher percentage of this inherited disease, which is autosomal, recessive. Contrary to the X-linked hemophilia A, the autosomal, recessive von Willebrand disease can affect both male and female. In vWD, hemostasis cannot be easily achieved due to a lack of vWF, or functionality of vWF.[34–36] In severe cases of vWD, it can easily be mistaken for hemophilia A and therefore mistreated as such. This is especially dangerous as the lack of vWF can lead to low levels of FVIII as FVIII is not as stable without its partner and can be rapidly degraded by proteases; thus making hemostasis even more difficult.[37] Additionally, the symptoms of von Willebrand disease is so mild that those who are affected are unaware that they

have hemorrhagic difficulties.[38] Given that most cases are mild, a large majority of von Willebrand disease patients are treated with the on-demand administration of Desmopressin which stimulates the release of vWF.[39] In more severe cases however, IV infusions of vWF are often required.

There are three types of von Willebrand disease, two of which are quantitative and one of them being qualitative. Von Willebrand disease Type 1 and type 3 are quantitative disorders where the body does not produce sufficient levels of vWF. Type 1 is where the body produces an unusually low amount of vWF. This is the most common form of the disease, approximately 75% of cases seen are type 1 and they are usually very mild in nature.[40] Type 3 vWD is the rarest and most severe form of the three disorders where the body fails to produce any viable vWF, thus leading to borderline non-existent levels of fVIII.[41] Lastly, vWD type 2, is a qualitative disease that affects vWF's ability to associate properly to other proteins of interest. There are four subcategories of type 2 vWD: 2A, 2B, 2M, and 2N.[42] Each of these subcategories involve a gene mutation that affects vWF's ability to properly bind to its various associated partners, and therefore affecting hemostasis. Type 2N, also known as the Normandy type, is the von Willebrand disease of interest in this study. Type 2N is caused by the inability of vWF to associate to FVIII and thus presenting similarly as hemophilia A and its respective levels of FVIII in circulation.[43]

**Introduction to von Willebrand Factor**

As mentioned previously in chapter 1, von Willebrand Factor serves as an important part to the coagulation cascade to promote hemostasis. In the event of an injury, vWF binds to the subendothelial collagen through its A3 domain, followed by binding to the inactive platelets via its A1 domain to the platelet glycoprotein (GP) receptor; thereby recruiting additional platelets to the site of injury.[44] Additionally, vWF also serves the important role as FVIII's circulatory partner to ensure FVIII's stability in circulation. An estimated amount of 95% of FVIII in circulation is partnered with vWF, the partnership between the two proteins prevents proteolytic cleavage during circulation. Furthermore, the vWF:FVIII complex prevents premature association of FVIII to FXIa or activated platelet.[45,46] The importance of the protein-protein interaction have proven to be evident in the severity of vWD type 2N and 3; where the body produces normal level of FVIII but often rests at hemophiliac's level due to the body's inability to effectively bind to vWF.

Von Willebrand factor (vWF) is a 2,050 residue glycoprotein that is mainly produced in endothelial cells and megakaryocytes.[47,48] This protein is synthesized with 2,813 residues, including 22 amino acid signal peptides followed by a 741 residue propeptide (D1 and D2) that is later proteolytically cleaved.[47] VWF was previously known to be synthesized with the arrangement of D1-D2-D'-D3-A1-A2-A3-D4-B1-B2-C1-C2-CTCK (Figure 9).[47–51] However, further studies of sequence and structure of vWF indicated heightened complexity than initially sought with complex assemblies that lack hydrophobic cores but are connected via extensive disulfide linkages.[52] Given that there are multiple domains, vWF will be briefly discussed by their associated domains alphabetically. The three A domains are large and globular in

comparison to the D domain. The A domains are also the only domain in vWF that lack an abundance of cysteines in comparison to the rest of the domains. The B and C domains have also been annotated in certain studies as six tandem von Willebrand C (vWC). The vWC-like domains are followed by the C-terminal cysteine knot (CTCK) domain.[53] Recent studies have shown that the D domains are consists of smaller modules, also known as the vWD domain, cysteine-8 (C8) domain, trypsin inhibitor-like (TIL) domains, and E domains.

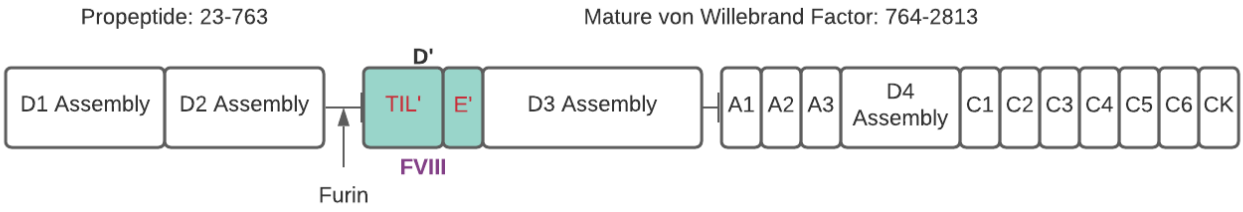


Figure 9. VWF Schematic (adapted from Dagil et al. 2019): domain arrangement of full length vWF. Propeptide composed of the D1 and D2 assembly followed by a furin cleavage site prior to the D' domain. The D' domain is also composed of two separate domains, the TIL' and E' domains, highlighted in light green where FVIII binds (indicated in purple). The D' domain is the opening domain for mature von Willebrand factor.[54]

The primary FVIII binding site on vWF is located in the D'D3 domains (Figure 9).[54,55] Recent studies have shown that the D' domain is most involved and responsible for binding to FVIII. The D' domain is composed of two components, the trypsin-inhibitor-like domain (TIL') and the E' domain (Figure 9).[56] Previous studies on epitope mapping utilized anti-vWF monoclonal antibodies along with a large percentage (approximately 72%) of missense mutations leading to type 2N vWF are located in the TIL' domain.[57] A previous solution structure of independent TIL'E' published in 2014 by Shiltagh et al. provided information regarding the D' domain's dynamicity and its involvement in FVIII binding (Figure 10).[56] The

authors proposed a binding mechanism in which the positively charged region in TIL' along with its inflexible scaffold in the E' region forms an electrostatic attraction with the acidic region of the A3 domain of FVIII. Furthermore, the A3 domain of FVIII has been proven to be critical for vWF binding, which makes this proposed interaction more feasible and worth studying.[56,58] As noted, the A3 domain of FVIII is the primary binding site for the D' region, however, studies have shown that full length vWF also involves binding sites in the C2 domain of FVIII.[59,60]

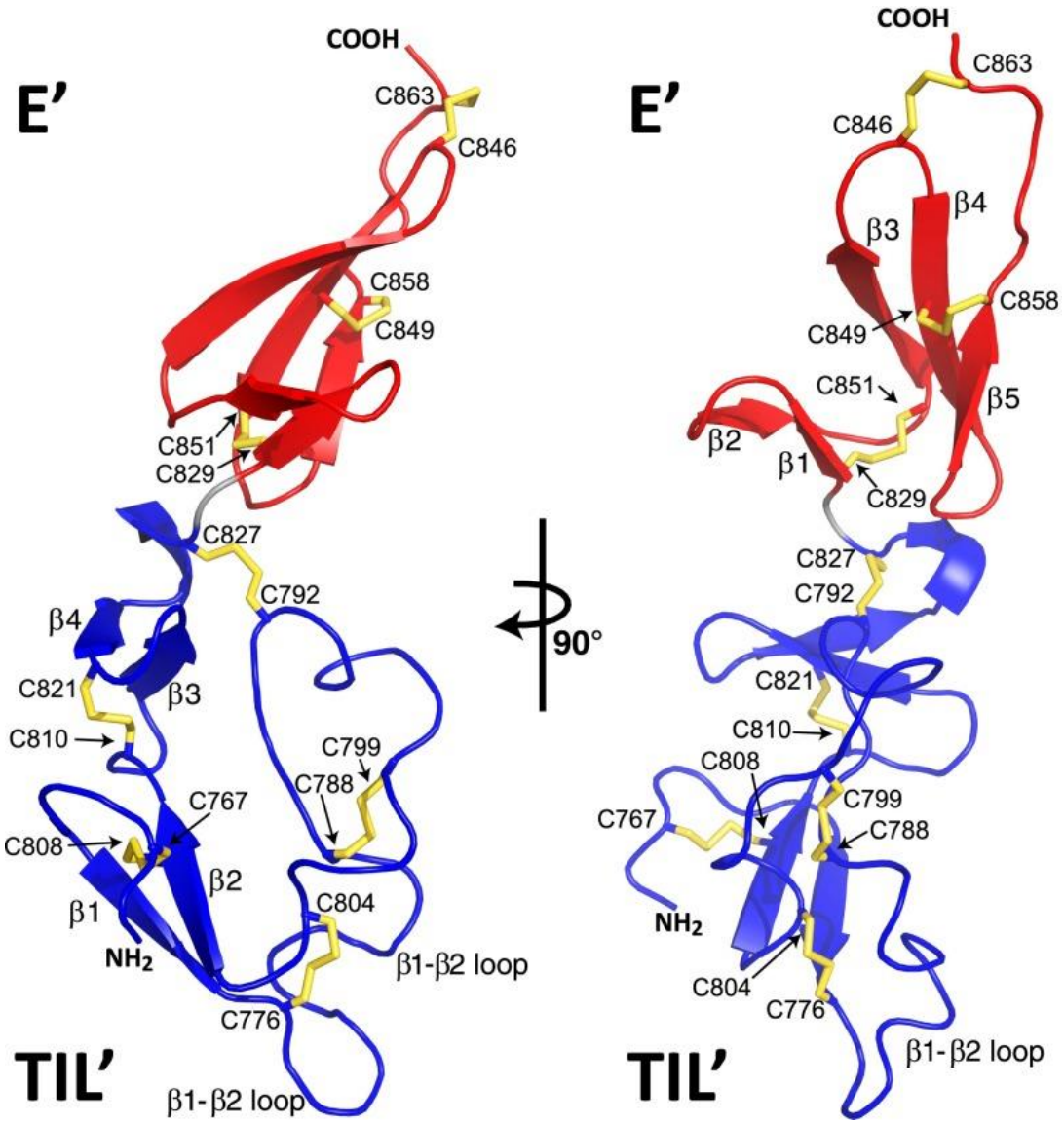


Figure 10. Solution structure of the D' (TIL'E') domain of vWF (PDB ID: 2MHP). The TIL' region is labeled blue and the E' domain is labeled red. Disulfide linkages are noted in yellow, and the beta strands are numbered in the order they present themselves in TIL' and E' domains independent primary sequences. It's noted that 70% of beta loops reside in the TIL' domain, and that the five conserved cysteines in the TIL' domain serve as its primary stabilizing force.[47] TIL' (blue) is formed of two ß sheets, ß1 and ß2 (residues 772-775 and 806-809, respectively), which then forms a scaffold containing a long 30 residue loops, ß1- ß2 loop. The ß1- ß2 loop involves an eight-residue gap between the second and third conserved cysteine residues (C776 and C804). The conserved cystines in the ß1-ß2 provides the TIL' domain with its intrinsic dynamic character.[22,56]

Crystallography of the isolated D' domain of vWF has proven to be difficult due to its flexibility.[56] Therefore, we attempted to co-crystalize the small fragment of vWF, TIL'E', in complex with the chimeric structure of FVIII, ET3i. During the continuous pursuit of the TIL'E':ET3i complex crystal trials, a recent publication revealed a high-resolution structure of FVIII:D'D3 complex via cryo-electron microscopy (Cryo-EM) (Figure 11). The 2.9Å structure of the FVIII:D'D3 complex was completed with a bioengineered clinical-stage FVIII molecule deemed BIVV001. Recombinant FVIII have proven to extend the half-life of FVIII in circulation, though most FVIII products are constrained to an 18-19 hour ceiling imposed by vWF-mediated clearance.[55] The novel BIV001 designed and utilized in the high resolution crystal structure consisted of a single-chain human B domain-deleted rFVIII, two IgG1 $F_c$ domains, D'D3 domains of vWF, and two XTEN polypeptide linkers. This bioengineered FVIII was designed to overcome the vWF-mediated half-life ceiling. In other words, the novel BIVV001 resulted in a stabilized rFVIII-D'D3 complex.[55] The structure showed sulfated FVIII-a3 Y1680 interacting directly with the side chain of TIL', R816, and mutations in either residue may cause disease (Figure 12). Mutations on Y1680 may cause severe hemophilia A, and mutations on TIL' in vWF may cause some of the most severe forms of vWD type 2N (Figure 13). Thus, supporting the significance of proper binding between the two residues.[58] Most importantly, the complex structure further confirmed the long proposed binding hypothesis made by Smith et al: the TIL' domain interacts largely with the C1 and A3 domain via Van Der Waals interactions (Figure 14, figure 15). Notably, the FVIII a3 acidic peptide region established as a critical determinant of FVIII-vWF complex formation which inserts into a basic groove formed at the TIL'E' and rFVIII interface. Lastly, in contrast to previous studies and hypotheses made, the TIL' domain does not make any contacts with the C2 domain of FVIII.[55]

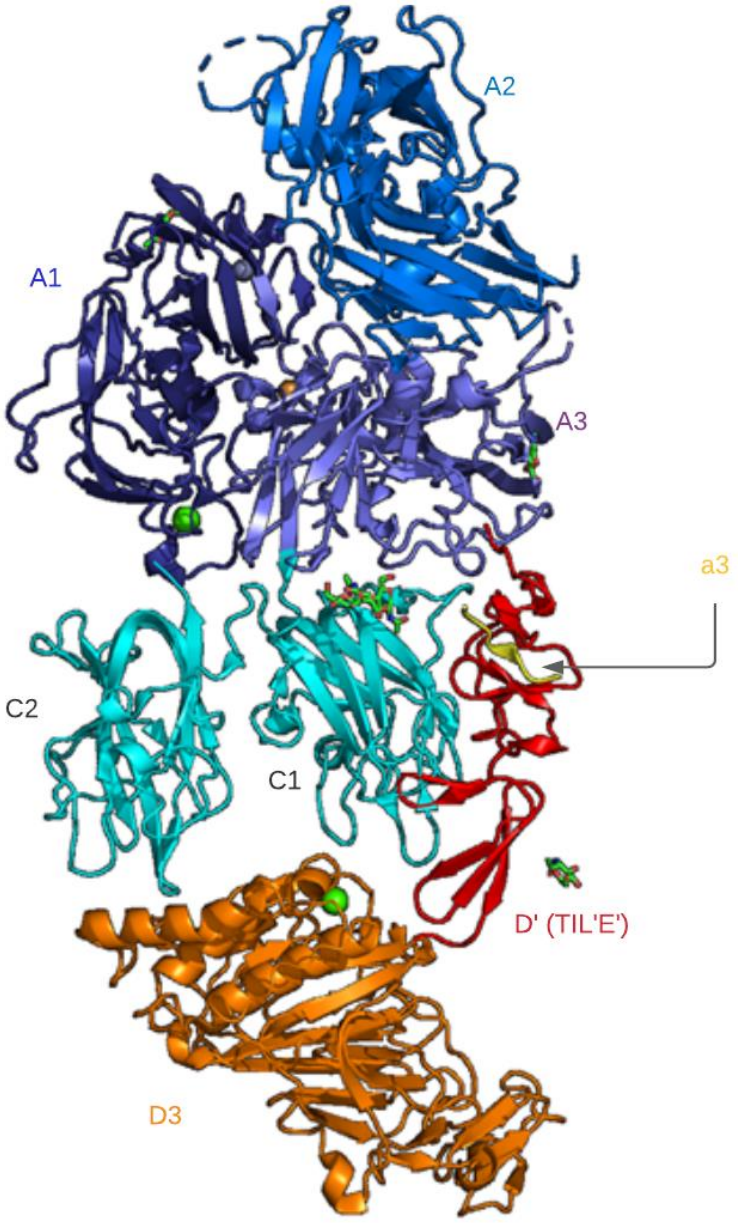


Figure 11. Cartoon representation of recently published crystal structure of FVIII:D'D3 (PDB ID: 7KWO). The C domains that observe structural homology are noted in cyan, and the A domains are noted in different shades of blue, D' of vWF is noted in red with direct interaction with the acidic a3 peptide (noted in yellow) as well as the C1 domain. The D3 domain of vWF is noted in orange;

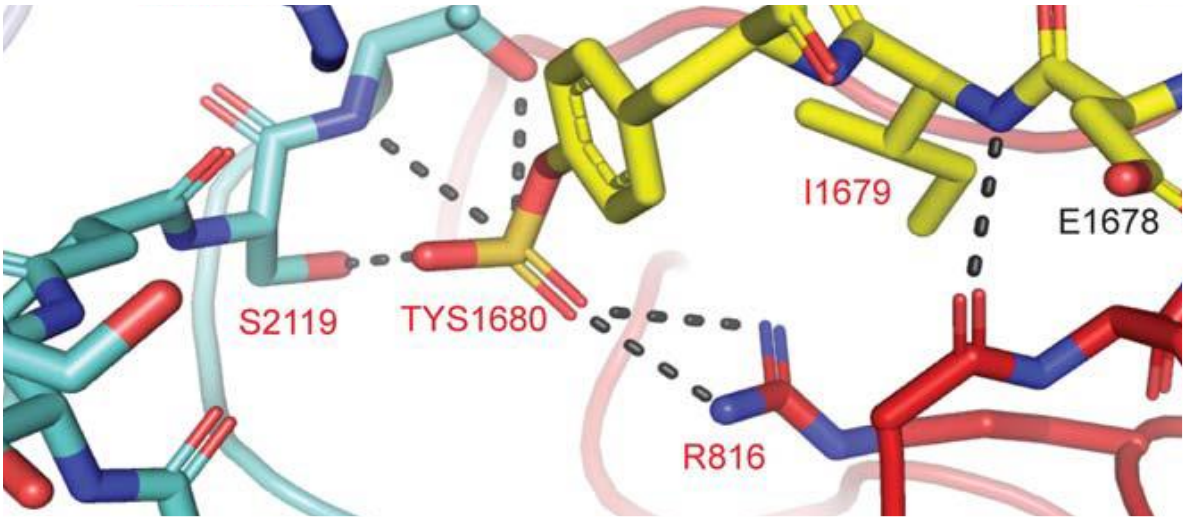

Figure 12. Figure of sulfated Y1680 noted in sticks (yellow), the side chain of TIL' R816 noted in red. The high-affinity electrostatic interaction noted in gray doted lines. Mutations noted to either residue would result in deleterious effects and cause severe forms of hemophilia A and vWD type 2N (adapted from Fuller et al. 2021).

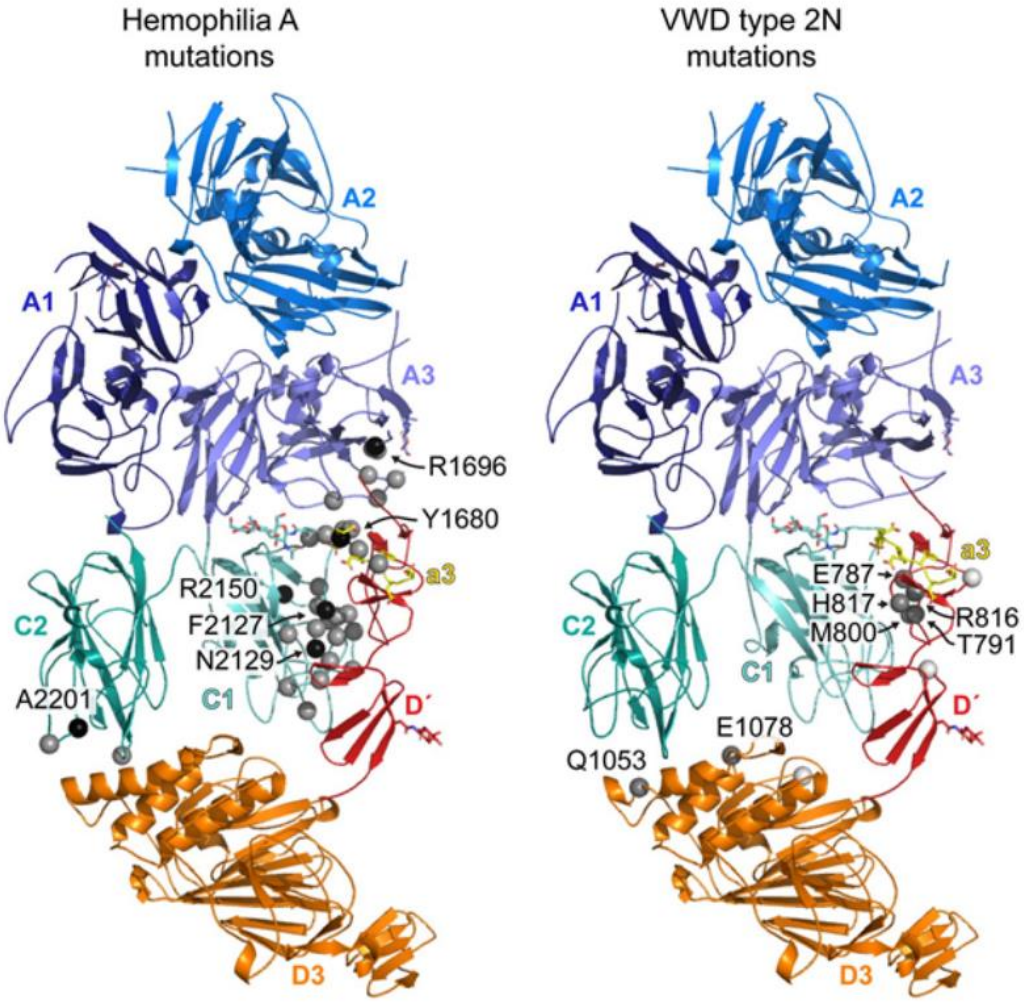


Figure 13. Mutations noted in FVIII (left) causes hemophilia A, specifically the mutations noted in the A3 and C1 domain. Mutations noted in vWF (right) causes von Willebrand disease, with a large majority in the D' domain (red) which causes type 2N vWF.

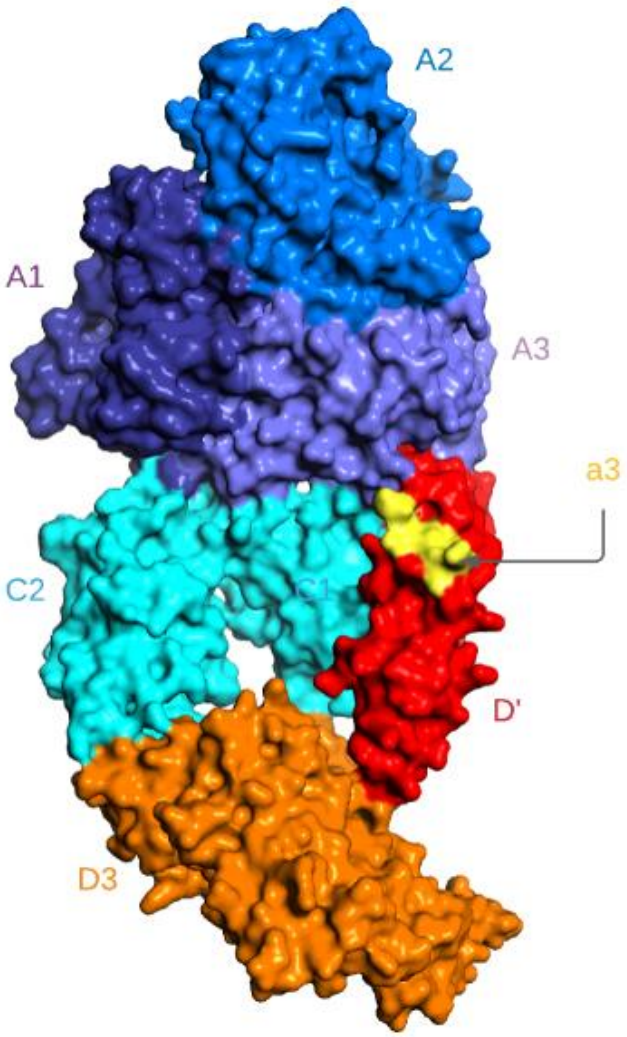


Figure 14. Electrostatic surface map of full length FVIII:vWF, colors are labeled depicting each domain. The a3 domain of FVIII has been highlighted yellow indicating the acidic binding pocket. TIL'E' is noted to engulf the a3 domain with electrostatic interactions as well as the N-terminus being docked into the A3 region's basic pocket.

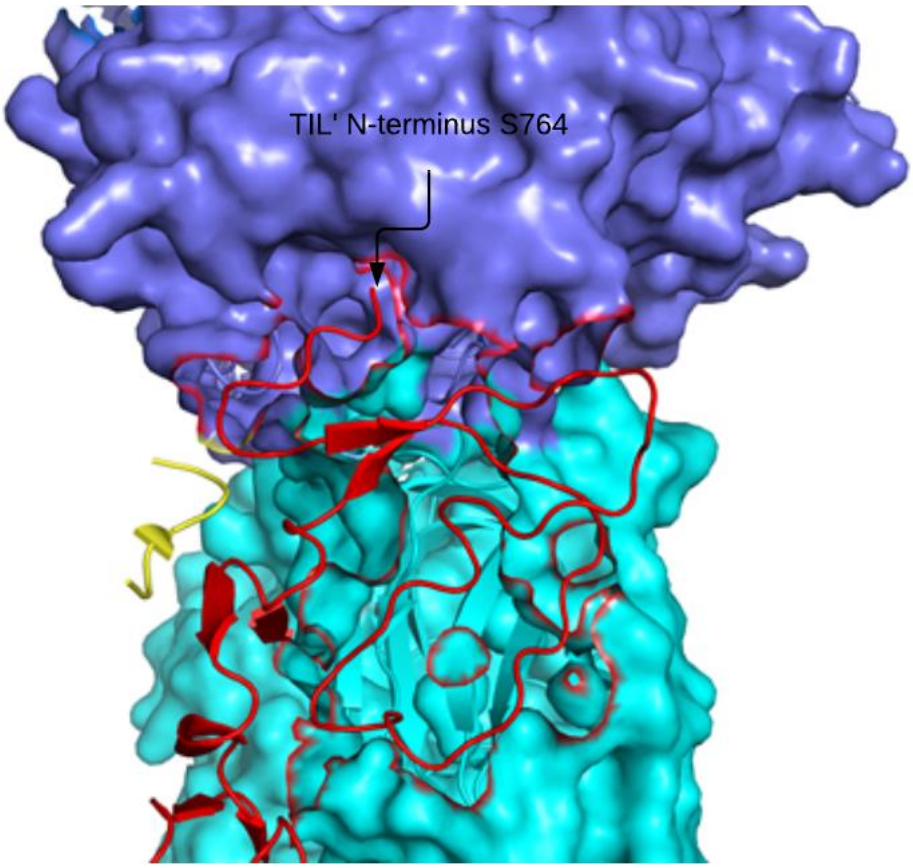


Figure 15. Figure of small pocket insertion of vWF TIL’ into the A3 domain (violet) shown in surface rendering with its shape complementarity to the C1 domain, noted in cyan. Insertion of vWF TIL’ (red ribbon) N-terminus S764 in a small and shallow pocket of the A3 domain is visualized here.

Lastly, the complex structure further verified the E’ domain of vWF being the connector between the TIL’ domain and the D3 domain; as it makes minimal contact with FVIII, and there are not many type 2N mutations documented in this region.

# Chapter 3

## TIL'E' Mutants Designs

The solution structure of TIL'E' as well as the recent cryo-EM structure of FVIII:vWF have allowed a magnitude of interpretation on type 2N vWD missense mutations. The most severe forms of type 2N vWD missense are noted in the TIL' region that affects binding to FVIII. In order to further understand some of the most documented missense mutations that cause severe type 2N vWD, detailed structural understanding along with binding mechanism is necessary. Site directed mutagenesis was employed in this present study to further understand the binding mechanism of TIL'E' to ET3i in addition to the recent FVIII:vWF structure. Up until the recent structure, the proposed binding mechanism has been the electrostatics interaction with the A3 domain of ET3i.[11,56] The most recent cryo-EM structure confirms the previous studies of FVIII/TIL'E' binding mechanism and its previously proposed docking system.[55] The primary binding region was noted in the TIL' domain of vWF, and mutations that cause changes in electrophobicity or hydrophobicity may affect binding and/or structural integrity and thereby affect its functionality. Therefore, the mutants selected have been previously documented to cause the omst severe forms of type 2N vWD. Three out of the four mutants were selected in the TIL' domain and one in the E' domain for further analyses (Table 1).

| | Mutation | Position | Hypothesis |
|---|---|---|---|
| TIL’ | R816Q | ß3 | Loss of conserved positive charge in the presumed A3 binding region |
| | E787K | ß1-ß2 Loop | Introduces positive charge in region of negative charge. Significantly decreases binding |
| | R782W | ß1-ß2 Loop | Loss of positive charge, change of polar to hydrophobic. |
| E’ | R854Q | ß4-ß5 loop | Loss of positive charge in FVIII anchor region |

Table 1. List of TIL’E’ mutations, position of the mutation in the TIL’E’ structure, and hypotheses of effects on binding to ET3i.

The mutations selected in the TIL’ domain include R816Q, E787K, and R782W; and R854Q in the E’ domain. No cysteines involved in any disulfide bonds were selected in this study as previous studies have shown multimerization, poor secretion, and reduced FVIII binding when cystine mutations were involved. This is due to TILL’E’ lacking a hydrophobic core, and the disulfide bonds involved in the structure serves as its primary stabilizing force. In other words, proper disulfide bond formation is necessary to the folding as well as function of vWF.[7] R816Q is located in the TIL’ domain of vWF, the mutation from arginine to glutamine creates a loss of conserved positive charged in the A3 binding region of FVIII (Figure 16). Given the proposed electrostatic interaction, the hypothesis of this mutant results in a decrease in binding affinity to FVIII. E787K and R782W are considered to be some of the more severe forms of type 2N phenotypes. The E787k mutation creates a positive charge in the binding protrusion, and thus likely would generate a significant disruption to binding to FVIII from a structural perspective. Furthermore, E787 along with R782 are in close proximity of the ß1-ß2 Loop where it is highly flexible, meaning that a missense may potentially involve a conformational change with

deleterious effect that significantly reduces binding to FVIII (Figure 17). R782W involves a mutation to tryptophan. This causes a change from the part hydrophobic and positively charged residue, arginine, to a neutral charge hydrophobic residue, tryptophan. The loss of the positively charge along with an increase in hydrophobicity may cause structural perturbation and significantly decreases binding to the putative A3 binding pocket (Figure 18). Lastly, the only mutation selected in the rigid E' domain, R854 with a mutation to a glutamine introduces a loss of positive charge (Figure 19). Though the E' domain does not make significant contact with the binding pocket of the C1 domain of FVIII, the mutation may affect how TIL' is connected to the E' domain of D'. The mutation may cause misfolding of the protein and therefore may poorly anchor itself to FVIII. The designed mutants were then compared to the binding of wild type (WT) TIL'E'.

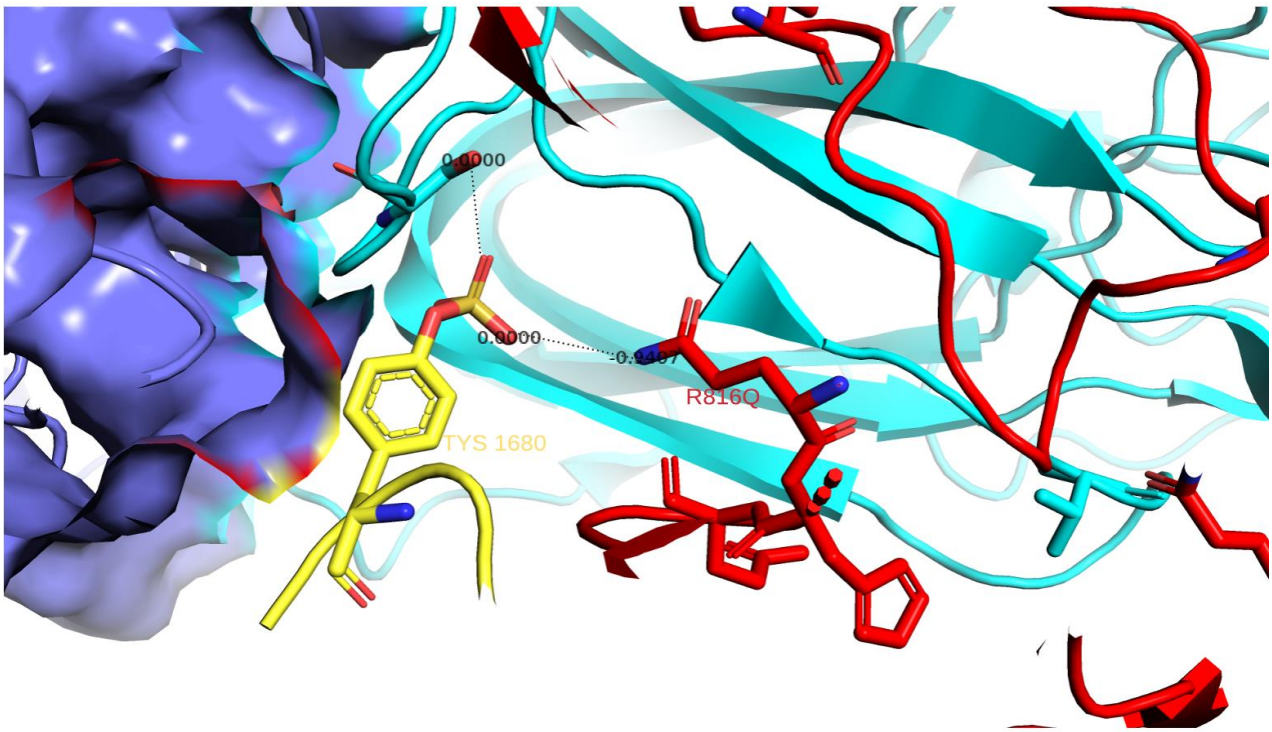


Figure 16. Stick representation of arginine mutation to glutamine at R816 (red). The mutation from an arginine to a glutamine introduces a loss of positive charge to the binding region of FVIII. This mutation has been documented to be one of the most severe forms of vWD type 2N

missense, and it's proposed to significantly reduce binding to the acidic region of a3, and therefore affects the high-affinity interaction with sulfated tyrosine at residue 1680.

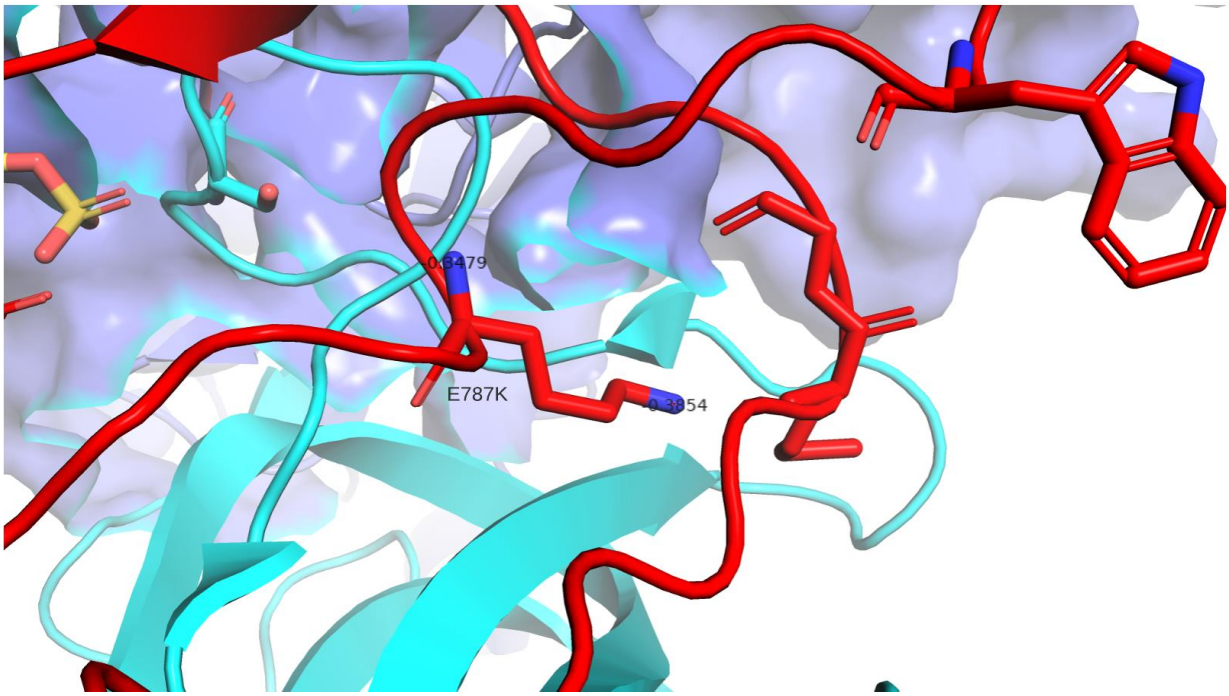


Figure 17. Stick representation of glutamic acid 787 mutation to positively charged Lysine (red). This mutation introduces an overall positive charge in a region within TIL' that is negatively charged and is hypothesized to affect proper disulfide formation of TIL' and thereby affecting its binding capabilities to FVIII. Overall charge of the residue is noted to be positive instead of the negatively charged wild type glutamic acid.

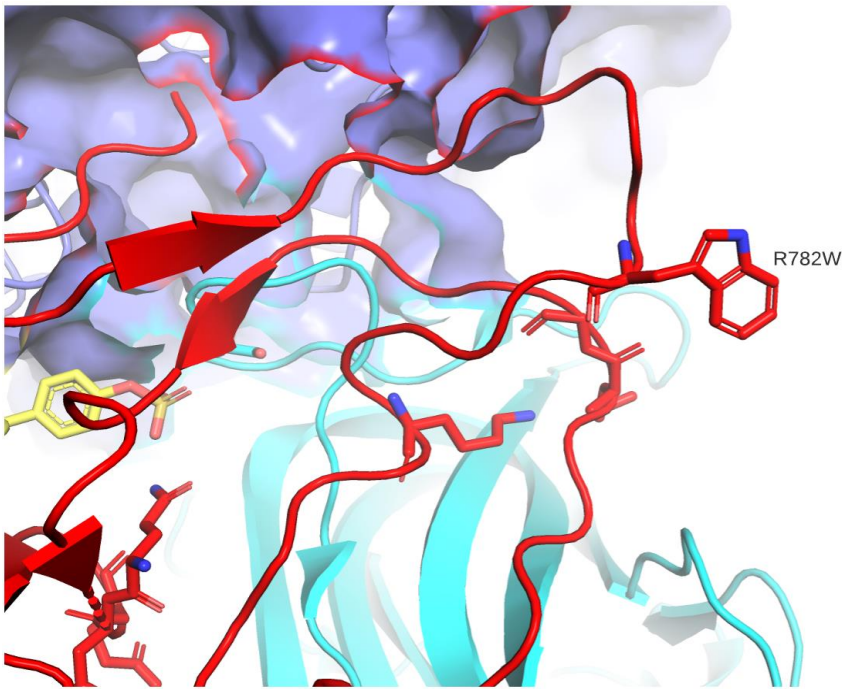


Figure 18. Positively charged Arginine 782 (red) mutation into hydrophobic and neutral tryptophan. This mutation may affect the proper folding of TIL' and therefore affecting its functionality.

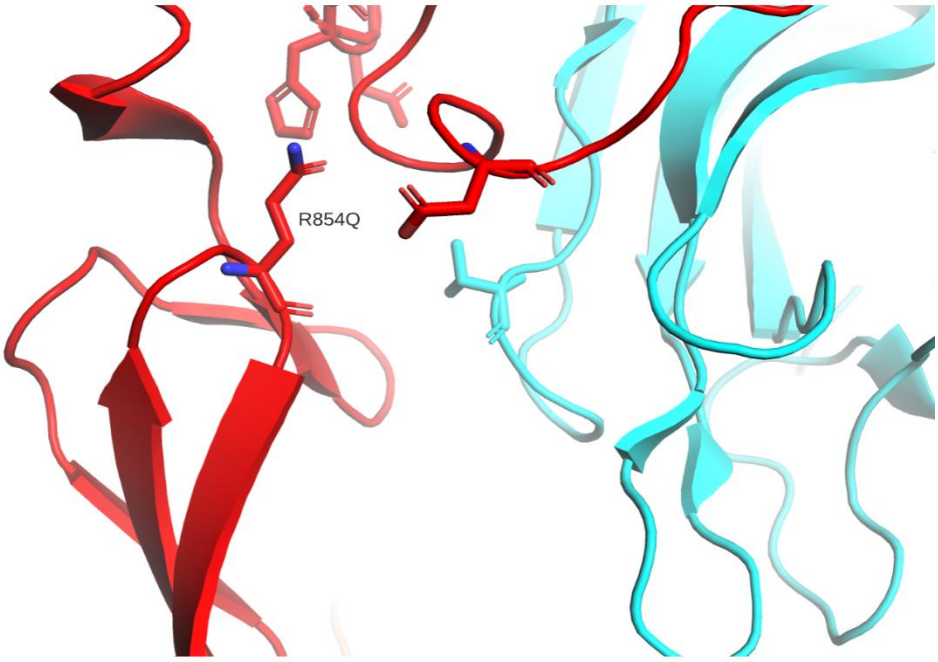


Figure 19. R854 located in the E' region has been reported to serve as an anchor into C1 domain of FVIII. Loss of positive charge from an arginine to a glutamine would affect its ability serve as a proper anchor to FVIII.

**Research Aim**

The goals of this present study include successful expression and purification of all mutants designed along with the wild type protein. Following successful purification of TIL'E' and its corresponding mutants, wild type TIL'E' in complex with our chimeric FVIII, Et3i, were formed for X-Ray crystallography attempts via hanging-drop vapor diffusion. Affinity pull-down assays were employed to assess binding between mutants and ET3i. Biolayer interferometry (BLI) was also employed to further study binding affinities to FVIII of all mutants in comparison to wild type. The aim of the BLI is to acquire quantitative data to further support and understand binding mechanism via $k_{on}$, $k_{off}$, and $K_D$ data.

# Chapter 4

## Materials and Methods

Wild type TIL'E' and each of the mutants described in chapter 3 were transformed, expressed, purified, proteolytically cleaved, and stored for future assays and crystallography trials. Binding assays conducted include biolayer interferometry, pull down assays, and sedimentation assays. Each portion of methods will be discussed in its corresponding section.

### DNA Plasmid Transformation of TIL'E' and Mutants

The pET32b(+) vector encoding the TIL'E' domain of vWF used in this present study was obtained from the Hansen Lab located in the University College London. This plasmid also encoded the thioredoxin (TRX) fusion protein tag along with the N-terminal internal $(His)_6$-tag. The protein and the $(His)_6$-tag are separated by a 31-residue linker protein and tobacco etch virus (TEV) protease cleavage site (Figure 20). Additionally, all mutants designed as mentioned in chapter 3 have adopted this schematic with single point mutations in its sequence. The TIL'E' mutant sequences were constructed utilizing the pET32b(+) vector with an ampicillin resistance site. The TIL'E' mutant plasmids were acquired from GenScript in lyophilized form and were transformed into chemically competent cell lines.

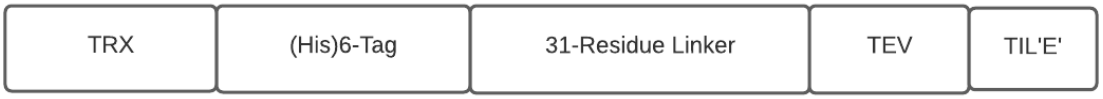


Figure 20. Schematic of expression product from TIL'E' plasmid obtained from Hansen Lab (University of College London). Construct depicts arrangement of the TIL'E'-TRX fusion protein utilized in this project.

Bioengineered chemically competent SHuffle® T7 B *E. coli* cells purchased from New England Biolabs (NEB) Inc. SHuffle® cell line was transformed with the pET32b(+) plasmids encoding the TIL'E' mutants. The cells were transformed following the optimized protocol provided by NEB, resulting in single colonies grown on LB Agar plates. Approximately 100ng of selected TIL'E' or TIL'E' mutant DNA were utilized and incubated with the T7 competent *E. coli* cells for 30 minutes on ice. The cells were then heat shocked at exactly 42$^{o}$C for 30 seconds, followed by a five-minute incubation on ice. One milliliter of room temperature Super Optimal Broth with Catabolite repression (SOC) medium was added, and the mixture was shaken at 250rpm for 60 minutes at 30$^{o}$C. The cells were then spread onto LB agar ampicillin$^{50}$ plates via sterile technique and incubated overnight at 30$^{o}$C. The overnight plate yielded multiple colonies of cells, and a single colony was harvested and grown for cell stock as well as large scale growth and expression.

**Large Scale Growth and Expression**

Ten milliliters of Luiria Bertani (LB) broth containing 10% w/v Bactotryptone, 5% w/v yeast extract, and 10% w/v sodium chloride were utilized as starter culture. These 10ml LB broths were prepared beforehand in bulk. The room temperature 10ml LB broths are then

inoculated with the selected colonies from the overnight plate along with amplicillin[50] (Amp) and are allowed to grow overnight at 200rpm and 30°C. The starter cultures were then utilized to inoculate 1L LB and Amp broths for large scale growth. The 1LB/amp broth are grown at 30°C until an $OD_{600}$ reading of at least 0.6 AU was reached, then the broth was induced with 400µl of 1M Isopropyl β-D-1-thiogalactopyranoside (IPTG). The temperature was then lowered to 15°C for overnight expression.

**Affinity Chromatography Purification**

The cells were harvested within 16-20 hours of expression at 15°C with the F12-6x500 LEX rotor from Thermo Scientific for 10 minutes at 6371 g-force and 4°C. The cell pellet was collected and resuspended in lysis buffer containing 20mM Tris-HCl (pH 7.5), 500mM NaCl, and 10mM imidazole along with 350µl of 1M phenylmethylsulfonyl fluoride (PMSF), and 700µl of 1M Lysozyme. This was followed by 35 minutes of incubation time on ice with gentle intermittent mixing of the resuspension. The resuspended cells were lysed via sonification using a Branson Sonifier 450 probe with a power output of five and duty cycle of 50% for one minute. In the event a larger cell pallet, a 30 second recovery time was applied between sonification. Cell debris was removed by a secondary high-speed centrifuge spin. The lysed cells were centrifuged at 17,000rpm in an F20-12x50 LEX Thermo Scientific rotor for 45 minutes at 4°C. The high-speed supernatant was filtered manually via a syringe with a 5µm filter. In a larger scale (6L-12L) growth, multiple 5µm filters may be required. In the event of clogging, a secondary 5µm filter was utilized for filtration prior to purification.

Immobilized metal affinity chromatography (IMAC) was employed for TIL'E' and TIL'E' mutant purification. 1ml of settled Ni-NTA Agarose resin obtained from Qiagen was used for 2L of *E. coli* cell growth. The resin is initially equilibrated into lysis buffer as mentioned above. The lysate was then flowed through it with a 15-minute incubation time along with intermittent agitation of the resin. The column was then washed twice with 20 column columns (CV) of wash buffers with increasing concentrations of imidazole, first 20mM followed by 40mM. The protein was finally eluted with 30 CV of elution buffer containing 20mM Tris-HCl (pH 7.5), 500mM NaCl, and 200mM imidazole. A gel sample was obtained for each of the wash steps and the elution step for sodium dodecyl sulfate-polyacrylamide gel electrophoresis (SDS-PAGE) verification. The fraction containing the most protein was then dialyzed in a 15 kDa molecular weight cut-off dialysis tubing by Spectrum Laboratories, Inc. overnight at 4$^{o}$C in dialysis buffer (20mM HEPES, 150mM NaCl, and 1% (v/v) glycerol).

**TEV Cleavage**

Tobacco etch virus (TEV) protease was utilized to cleave the TRX-$(His)_6$-tag-linker fragment from TIL'E'. A ratio of 1 $OD_{280}$ TEV to 10 $OD_{280}$ TIL'E' was utilized for this cleavage reaction. Samples containing the fusion $(His)_6$-tagged TIL'E' and TEV were incubated at room temperature for three hours, then was moved to 4$^{o}$C overnight for the completion of the cleavage reaction. The following day, a second nickel column was set up to capture the cleaved protein. Similar to the initial nickel column, the resin was initially equilibrated with lysis buffer followed by equilibration with the $(His)_6$-tagged TIL'E' with TEV to encourage binding of the $(His)_6$ trap with the resin. The resin was then washed with two separate 20 CV washes of 20mM and 40mM

imidazole, followed by the elution buffer. Once again, gel samples were obtained at each step for SDS-PAGE verification and efficacy of the TEV cleavage reaction. The very initial fraction (flow-through) was collected, concentrated, and buffer exchanged into HBS (storage buffer) via Amicon Ultra-15 Centrifugal filters (Ultracell 10K Millipore membrane). In the event where the volume is too much for buffer exchange, secondary dialysis would take place under the same conditions as the initial dialysis noted previously.

**Size Exclusion Chromatography**

Size exclusion chromatography (SEC) served as the final purification step for TIL'E'. TIL'E' was injected to a HiLoad$^{TM}$ 16/60 Superdex 75 (S75) preparatory grade size exclusion chromatography column by GE Healthcare. The column was washed with nanopure water prior to equilibration with HBS (storage buffer). The peaks on the chromatogram were further collected for SDS-PAGE analysis and confirmation.

**Affinity Pull-Down Assays (Ni-NTA Agarose Resin)**

Ni-NTA Agarose Resin by Qiagen was utilized for initial binding assays. TRX-$(His)_6$-tagged TIL'E' and tagged TIL'E' mutants were incubated in equilibrated 100µl of Ni-NTA resin at room temperature for 15 minutes to encourage binding. Following incubation, tagged TIL'E' was then transferred to a Costar Spin-X® centrifuge tube filters, 0.22µm pore CA, then was washed twice with 10 CVs of HBS (storage buffer) with intervals of 800 x g spins. Following the washes, an equimolar ratio of ET 3i was added to the resin, and the sample was incubated at

room temperature for 5 minutes to encourage binding. The resin was then washed once with HBS (storage buffer), then eluted with elution buffer. Gel samples were collected at each flow through, wash, and elution step for further analyses via SDS-PAGE.

**Affinity Pull-Down Assays (TALON Magnetic Beads)**

TALON Magnetic beads by TaKaRa was employed for affinity pull-down assays, and the magnetic beads were first removed out of its ethanol storage into nanopure, followed by equilibration into HBS (or whichever the protein was dialyzed and stored into). Following similar protocol as an IMAC, a 1:1 ratio of TIL'E' (TIL'E' mutants):ET3i was utilized for the binding assay. Approximately 15µg-30µg of TIL'E' was used and only 15µg of ET3i was used. Upon equilibration of the magnetic beads TALON resin, TIL'E' was incubated with ET3i without any disturbance of the resin for 15 minutes. The magnetic bead resin was then lifted aside of the Eppendorf tube via a strong magnet, and the flow through was extracted. The resin was washed twice with low imidazole content followed by a high imidazole elution buffer. Each column flow through, wash, and elution were extracted similarly with a strong magnet. Each column fraction collected was analyzed via SDS-PAGE.

**Liposome binding: Sedimentation Assays**

Anionic dioleoyl phosphatidylserine (DOPS) and zwitterionic dioleoyl phosphatidylcholine (DOPC) were utilized in sedimentation assays mimicking platelet binding. A 80:20 DOPS:DOPC ratio was utilized in each of the sedimentation assays, and the liposomes

were prepared in bulk and the stock liposomes are stored in -20$^{o}$C in argon gas. Six separate Beckman Coulter tubes (PC TK Wall 8x23mm) were made and they are labeled as ET3i:PC, ET3i:PSPC, TIL'E':PC, TIL'E':PSPC, ET3i:TIL'E':PC, and ET3i:TIL'E':PSPC. Each tube consists of their corresponding components with a final volume of 300µl (125µl of DOPC, 125µl of DOPS (80:20), 1:1 equimolar ratio of TIL'E' and ET3i, brought to final volume with nano pure water). The mixture was para-filmed and incubated at room temperature for one hour prior to high-speed centrifugation. The Beckman tubes were then spun at 16000 rpm for 45 minutes with Sorvall MX 150 Micro-ultracentrifuge by Thermo Scientific. The supernatant from each tube was decanted and cold acetone (-20$^{o}$C) was added for acetone precipitation, the supernatant samples were incubated overnight in acetone at -20$^{o}$C. Each of the pellets (both visible and poorly visualized) were resuspended and agitated in 4x loading dye and stored in -20$^{o}$C in preparation for SDS-PAGE analyses. The incubated supernatant tubes were then spun at 16000 x g for 15 minutes the following day. The supernatant of this centrifugation was decanted, and a 10-minute recovery time was allowed for excess acetone to evaporate. Loading dye was added and the sample was agitated on Vortex 2.0 for resuspension in preparation for SDS-PAGE analyses.

**Biolayer Interferometry**

Biolayer interferometry (BLI) was selected as the quantitative evaluation of binding between ET3i, wild type TIL'E' and TIL'E' mutants. The bioengineered chimeric structure of FVIII, ET3i was obtained from our collaborators, Dr. Christopher Doering and Dr. Gabriela

Denning. BLI was accomplished with Pall ForteBio® BLITz instrument along with the BLITz Pro software. Anti-hC2 monoclonal antibody ($M_{AB}$) G99, prepared by previous lab members, was complexed with ET3i. This complex was incubated on ice for at least 15 minutes to encourage binding to each other. Upon initiation of the binding assay, a blank was taken where the anti-mouse tip (AMC) is soaked in HBS. Anti-C2 MAB G99:ET3i was then bound to AMC tips during the loading step, followed by another blank in which the buffer soaks away excess complex that did not bind to the tip. TIL'E' and each TIL'E' mutant was then associated to the tip followed by a dissociation step. The data set was then extracted from the Blitz program and processed initially in excel to ensure that the background has been subtracted off. The processed data were then further analyzed on GraphPad Prism 8.0 where a nonlinear regression curve was applied to the binding data. $k_{on}$, $k_{off,}$ and $K_D$ values were obtained via GraphPad Prism.

**X-Ray Crystallography**

Hanging drop vapor diffusion was employed to crystalize the ET3i:TIL'E' complex. Suitable conditions were acquired via large scale screens through Hauptman-Woodward Medical Research Institute; a select few conditions were further pursued. A total of 400µl were pipetted into each of the 24 well plates. Each well was manually greased for proper sealing upon placing of the glass slide. One microliter of the protein complex (ET3i:TIL'E') and 1µl of the well condition was pipetted onto the glass slide. The glass slide is then momentarily placed on top and over its corresponding well condition, this is repeated for all 24 wells. The crystal trays were left undisturbed for at least 24 hours to encourage vapor diffusion. Each tray was evaluated under

microscope to check for crystal formation. Multiple trays were made with differing buffer concentrations, pH levels, salt levels, precipitants, and polyethylene glycol (PEG) concentrations which will be discussed in the results and discussion section.

# Chapter 5

## Results and Discussion

### Preparation of pure Wild Type TIL'E' and TIL'E' Mutants

Wild type TIL'E' and its mutants were expressed and purified for further studies as well as crystal trials. Bacterial expression was employed in this study, TIL'E' and TIL'E' mutant plasmids were individually transformed into the New England Biolabs (NEB) bioengineered SHuffle *E. coli* cell line to aid in proper disulfide bond formation. To further encourage proper folding of disulfide bonds within D', the plasmid was designed to contain a N-terminal thioredoxin (TRX) tag (Figure 20).

Upon successful protein expression and harvest, a three-step affinity chromatography with Ni-NTA Agarose was employed to ensure sufficient protein purity. The first Ni-NTA (1$^{st}$ Nickel column) was utilized to separate a large majority of impurities from TIL'E' post protein expression. The column was washed with two low imidazole-containing buffers with a high imidazole elution. Upon collection of each of the gravity flow columns, the purity of the fractions was analyzed via SDS-PAGE (Figure 21). As seen in the initial nickel column, the tagged TIL'E' fusion protein migrates near 27kD. Some impurities are seen in the higher molecular weight region.

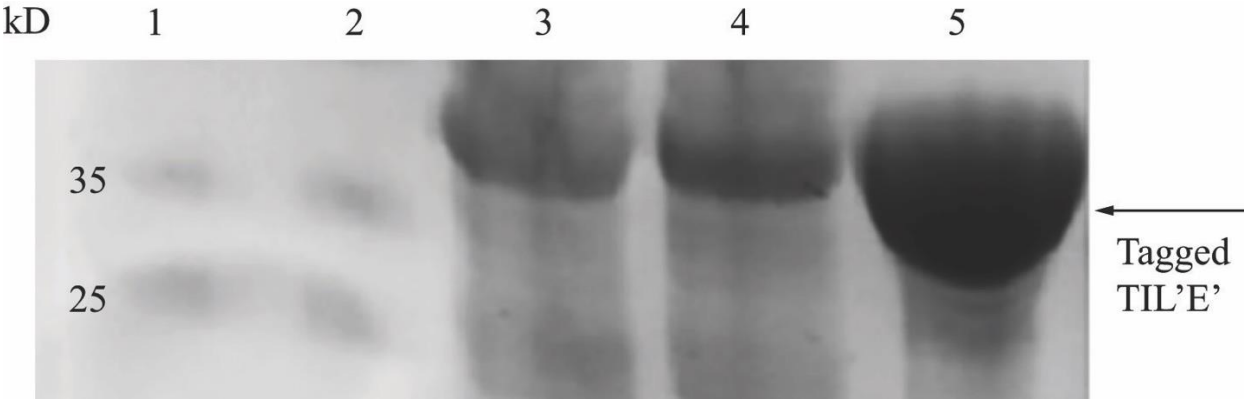


Figure 21. SDS-PAGE analysis and verification of TIL'E' protein purity following 1st nickel column. Lanes: 1. Molecular weight protein ladder; 2. Molecular weight protein ladder (due to lane leakage); 3. Filtered lysate flow through; 4. Column wash; 5. Elution fraction.

Following the initial nickel column, the fraction with the highest amount of protein was dialyzed out of imidazole and into the HBS buffer. A 2nd Ni-NTA column was employed to remove the TRX and $(His)_6$-tag-linker fragment via tobacco etch virus (TEV). All components along with tagged TIL'E' was collected in the 2nd nickel column (Figure 22). It can be visualized that there is some tagged TIL'E' remaining near 27 kD, along with TRX protein near 17kD and cleaved TIL'E' at 11kD. There is one contaminating band noted near 60 kD, and size exclusion chromatography was employed to purify TIL'E' further. SDS-PAGE verified pure and cleaved TIL'E' post SEC (Figure 23 and figure 24).

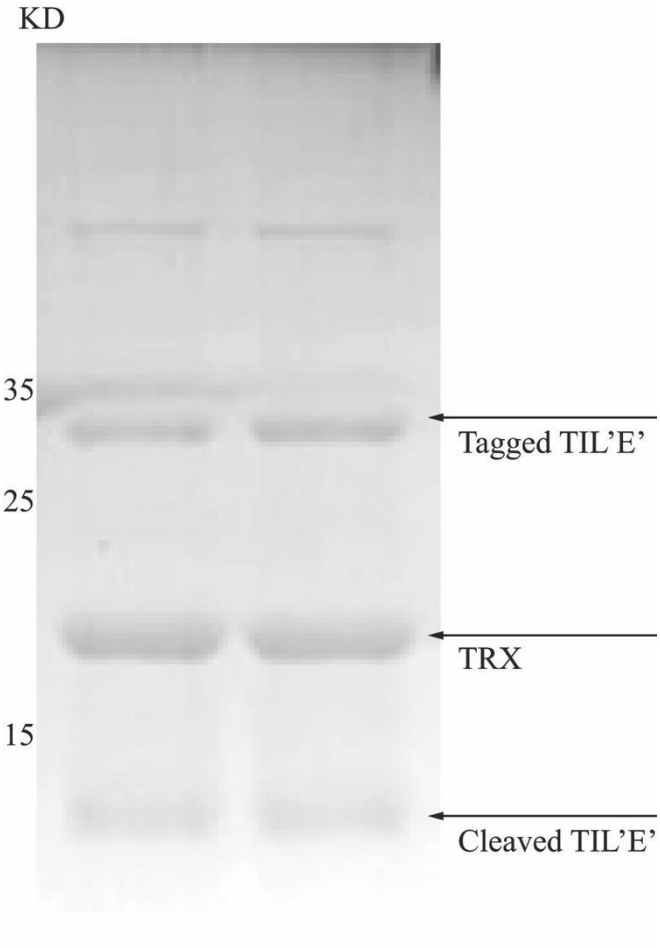


Figure 22. SDS-PAGE analysis post TEV cleavage of TIL'E'. Undigested (incomplete TEV digestion) Tagged wild type TIL'E' eluting at 27kDa, thioredoxin upon digestion eluting at 17kDa, followed by cleaved TIL'E' at 11kDa.

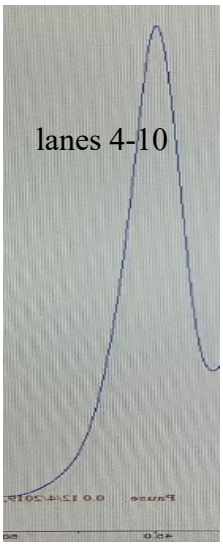


Figure 23. SEC Chromatogram for cleaved TIL'E elution fractions 4-10, as seen on SDS-PAGE verification in figure 24.

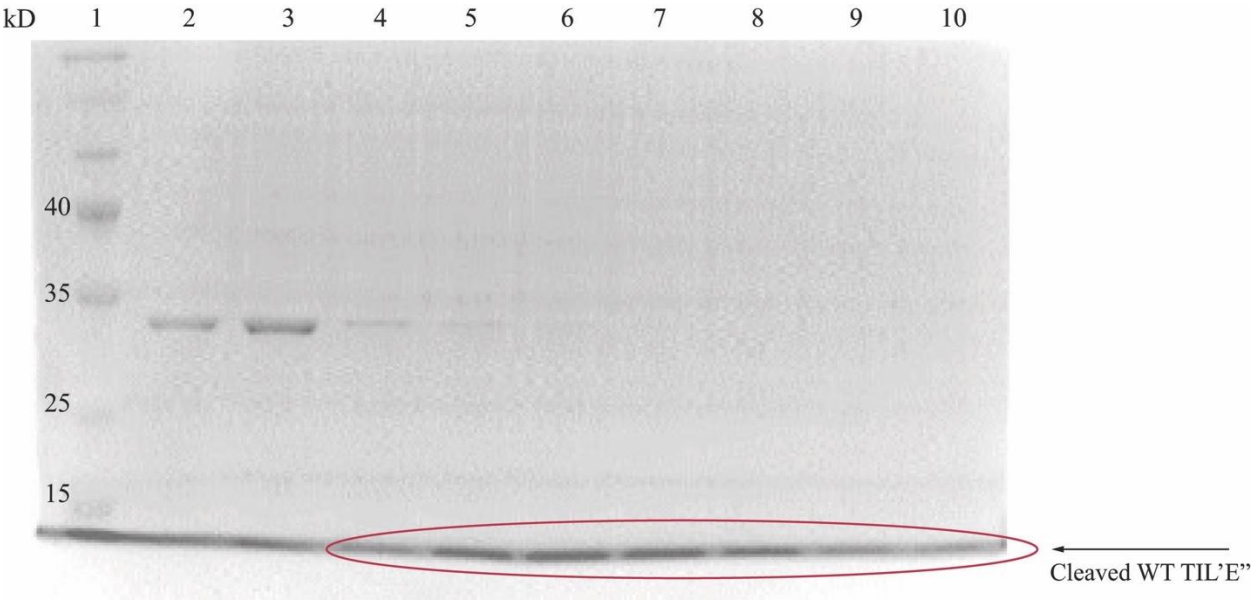


Figure 24. SDS-PAGE analysis post size exclusion chromatography (SEC). A. Elution profile of TIL'E' with highest peak being collectable fractions. B. Lanes: 1. Molecular weight protein ladder; Lanes 2-3: incomplete digestion of tagged TIL'E'; Lanes 4-10: Pure cleaved TIL'E' collectable fractions.

**R816Q, R782W, E787K, and R54Q (TIL'E' Mutants) Purification**

As mentioned previously, each of the mutants were designed adopting the same sequence as wild type TIL'E': TRX fusion protein-$(His)_6$-tag-linker. Each of the mutants contain a point mutation in its corresponding amino acid sequence. The same purification and cleavage method, immobilized metal affinity chromatography (IMAC) and TEV cleavage, respectively. SDS-PAGE analyses indicated relatively pure TIL'E' mutants. There were certain mutants that required secondary IMAC purification for contaminant removal, SDS-PAGE verified post purification yielded pure mutants (Figure 25-figure 28).

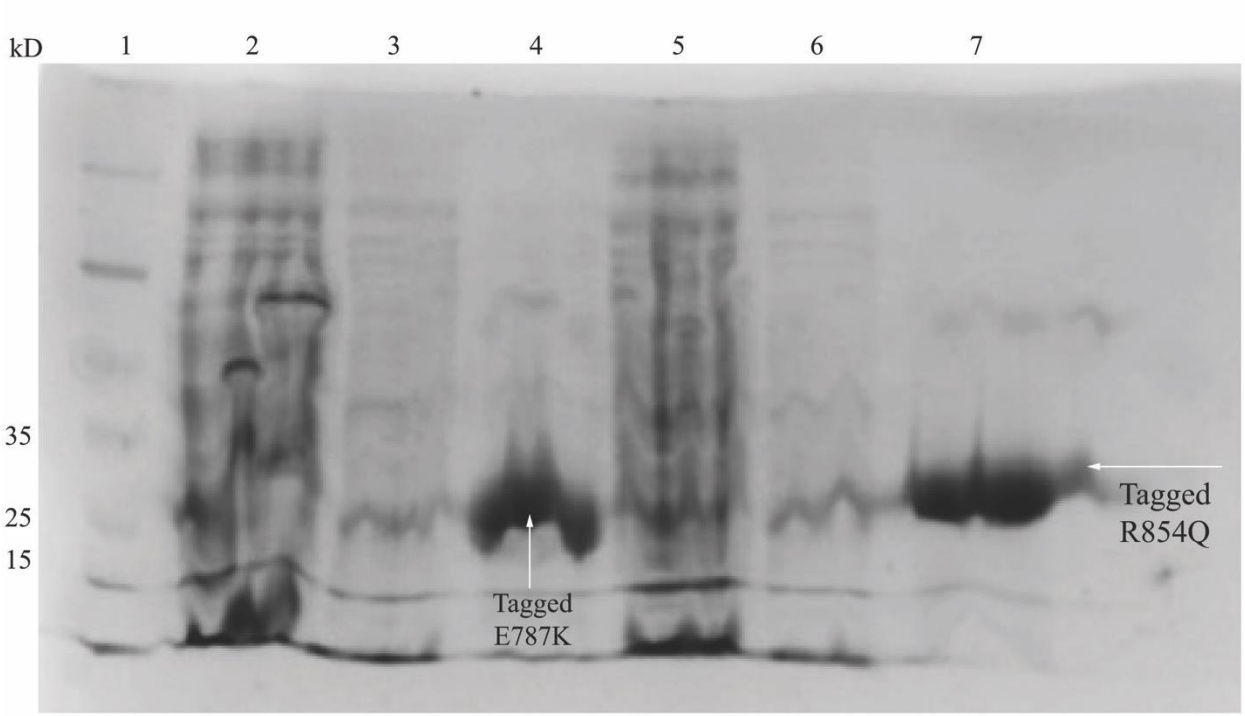


Figure 25. SDS-PAGE purification of E787 and R854Q. Lanes: 1. Molecular weight protein ladder; 2. E787K Initial lysate flow through; 3. E787K Wash column; 4. E787K Elution column; 5. Initial R854Q lysate flow through; 6. R854Q wash column; 7. R854Q elution column.

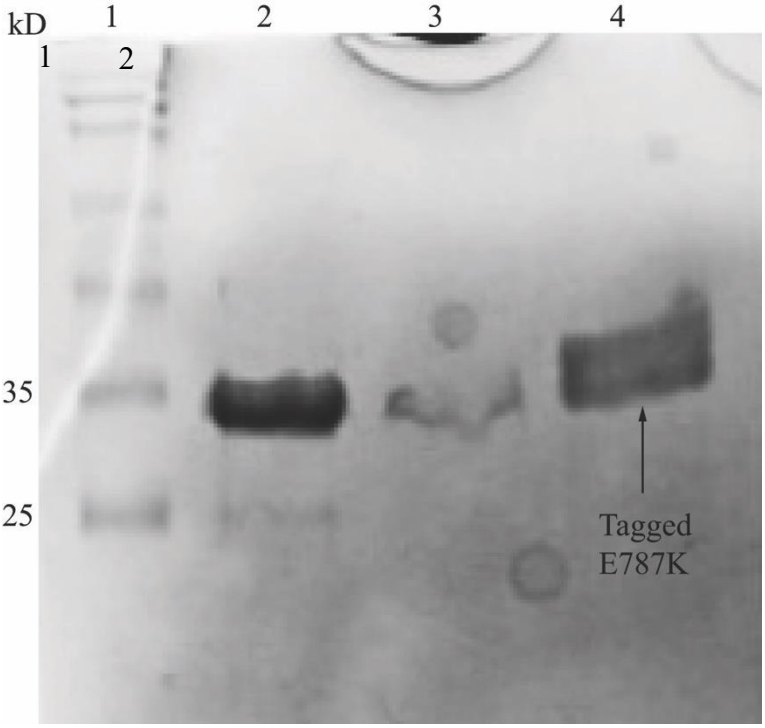


Figure 26. SDS-PAGE verification of E787K secondary IMAC. Lanes: 1. Molecular weight protein ladder; 2. Tagged E787K initial elution fraction (buffer exchanged into HBS); 3. E787K wash; 4. E787K elution fraction.

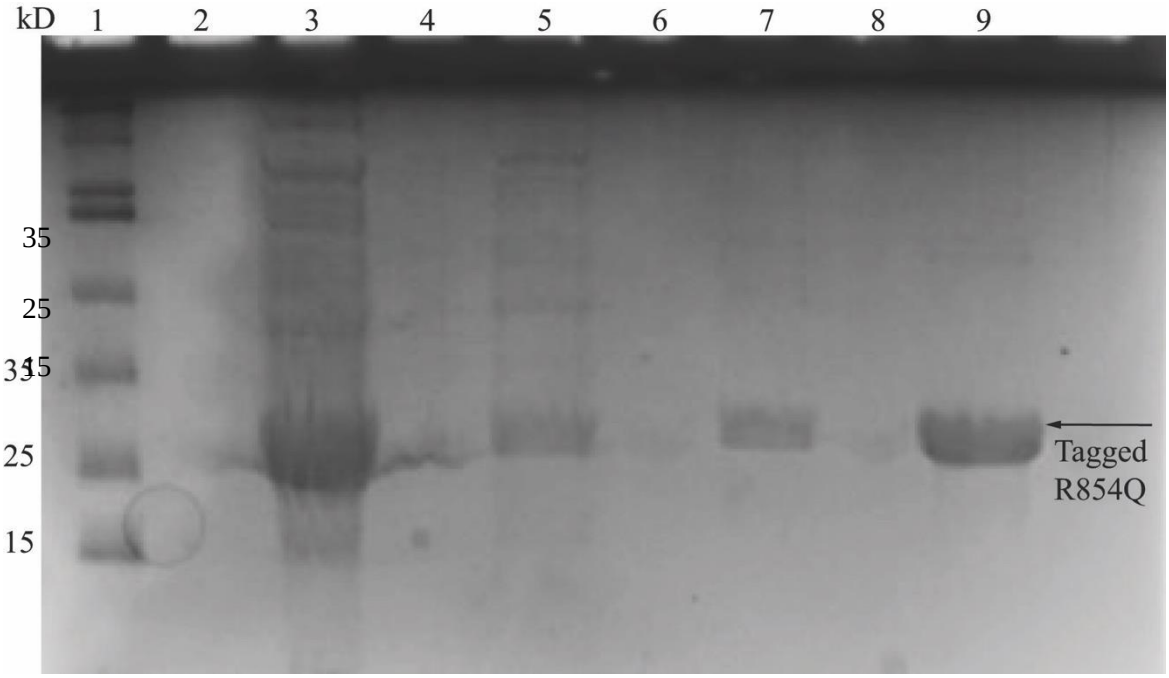


**Figure 27.** SDS-PAGE verification of R854Q secondary IMAC purification. Lanes: 1. Molecular weight protein ladder; 2. Intentional space; 3.R854Q lysate flow through; 4. Intentional space; 5. R854Q wash #1 (10mM Imidazole); 6. Intentional space; 7. R854Q wash #2 (40mM imidazole); 8. Intentional space; 9. Tagged R854Q elution fraction.

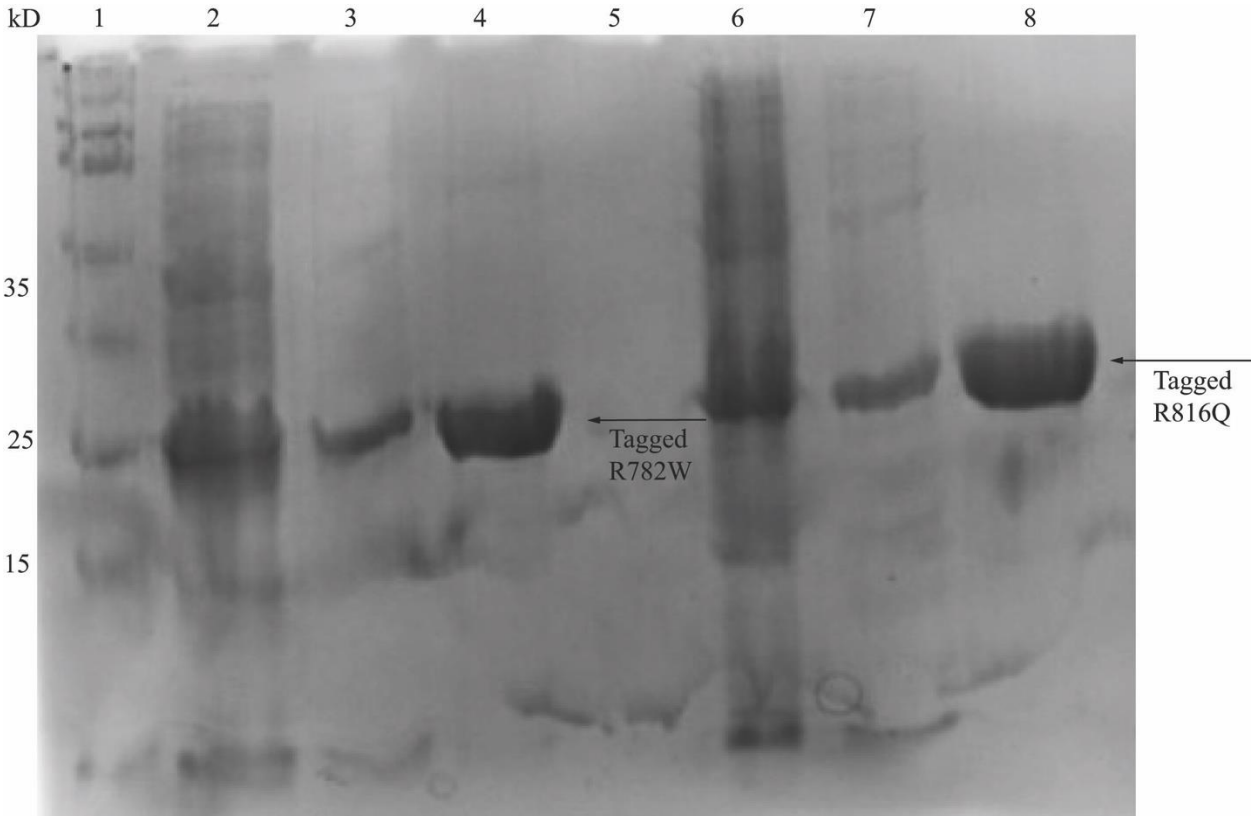

Figure 28. SDS-PAGE verification of tagged R782W and R816Q. Lanes: 1. Molecular weight protein ladder; 2. Initial R782W lysate flow through; 3. R782W wash column; 4. R782W elution column; 5. Intentional space; 6. Initial R816Q lysate flow through; 7. R816Q wash column; 8. R816Q elution column.

**Biolayer interferometry Binding Kinetics**

Previous studies have hypothesized electrostatic interaction between TIL'E' and FVIII in the a3 domain of FVIII and the TIL' domain of D'. As mentioned previously, during the composition of this project, a high-resolution complex cryo-EM crystal structure confirmed the Van Der Waals interaction the D' domain of vWF has on the a3 and A3 domains of FVIII. To further study the interaction between FVIII and TIL'E' in a quantitative manner, biolayer interferometry was employed. Serial dilutions of TIL'E' with HBS was made (2x dilution),

triplicate experiments were conducted for wild type along with each of the mutants to gather a series of data sets for analyses. To successfully bind TIL'E' to FVIII, an Anti-Mouse IgG $F_c$ capture (AMC) was utilized with monoclonal antibody (MAB) of choice, G99, in complex with ET3i. G99 has a reported binding affinity to FVIII of 15.5nM.[53] A 1:1 ration was employed for the G99:ET3i complex (Figure 29). The mixture was incubated for at least 15 minute to encourage binding. Following the protocol provided by Blitz, total of five sets of triplicate data was acquired. Each of these raw data sets were processed through excel to normalize the background data. Following background normalization, the data sets were processed once again with GraphPad Prism 8.0 for $k_{on}$, $k_{off}$, and $K_D$ quantification (Figure 30 and Table 2). Quantification data indicated decrease in binding with decreasing concentrations of TIL'E' in complex with G99:ET3i, which was expected.

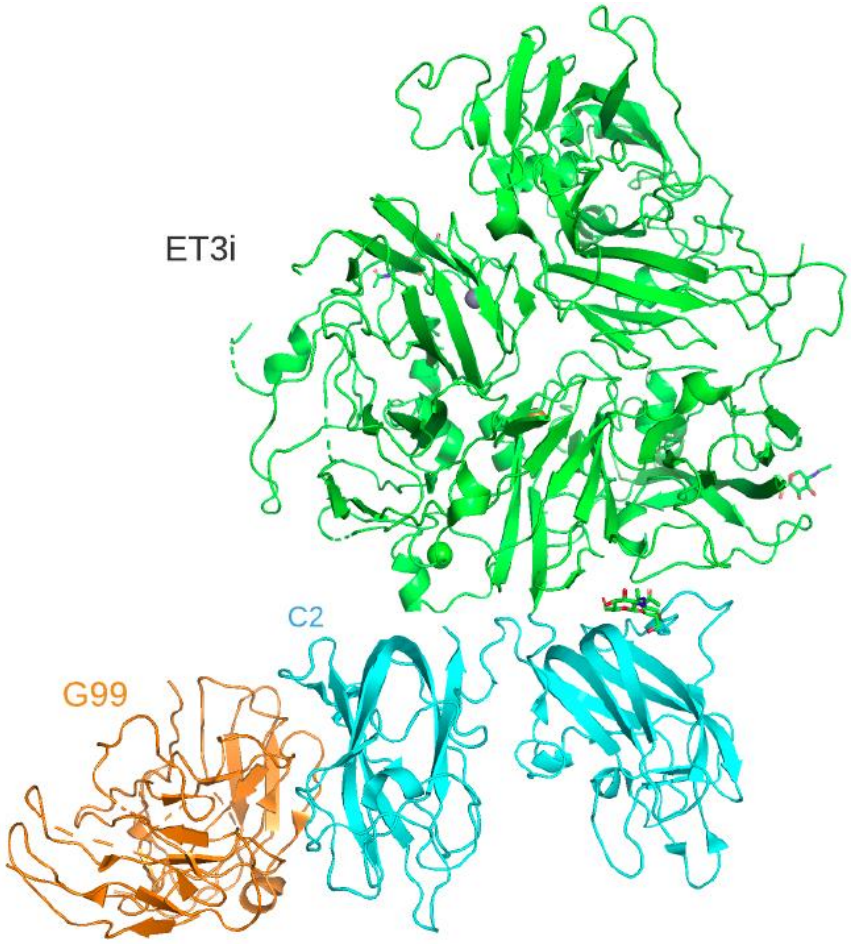


Figure 29. Schematic of the G99:ET3i complex utilized in BLI experiments. G99 (orange) binding to the C2 domain of FVIII (cyan).

A

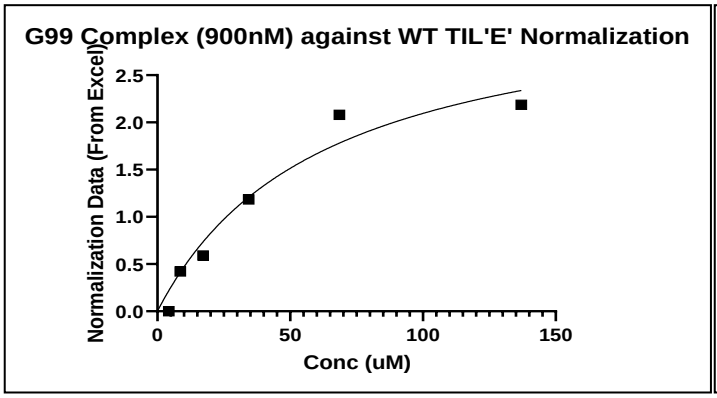


B

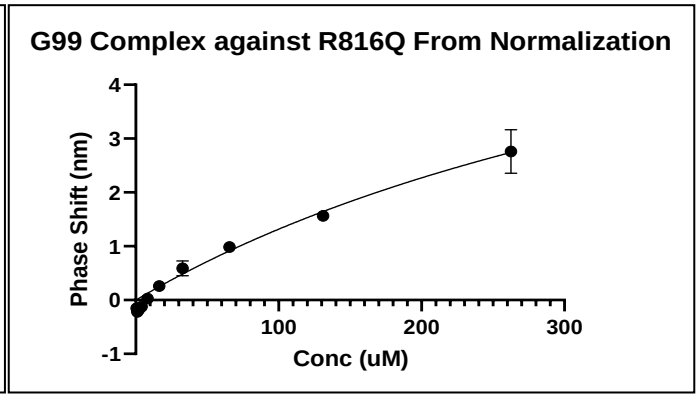


C

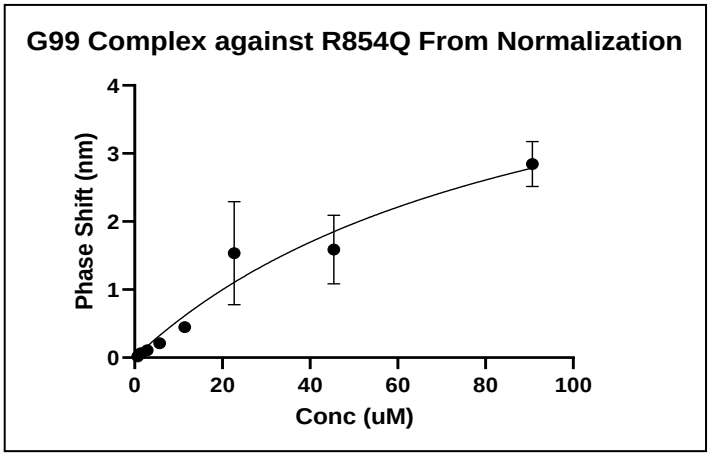


D

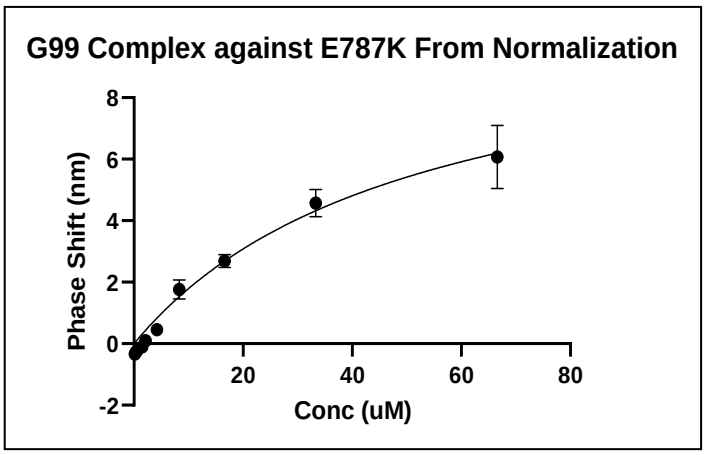


E.

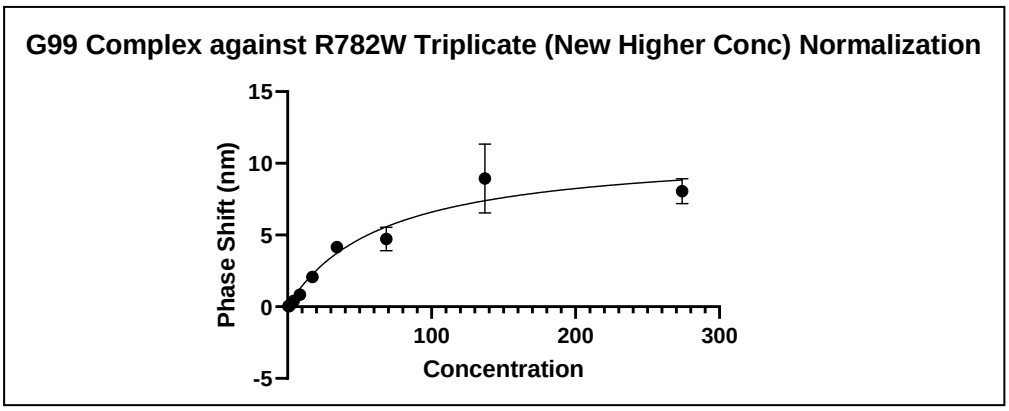


Figure 30. Non-linear regression curves for WT TIL'E' along with each of its mutants. The graph presented is an averaged data set from triplicate experimentations with normalization (subtraction of background). A. G99:ETi3i:WT TIL'E' with an initial TIL'E' concentration of 137µM. B. G99:ET3i:R816Q with an initial R816Q concentration of 262.6µM. C. G99:ET3i:R854Q with an initial R884Q concentration of 90.7µM. D. G99:ET3i:E787K with an initial concentration of E787K of 66.6µM. E. G99:ET3i:R782W with an initial concentration of

R782W of 274.1µM. Both WT TIL'E' along with each of the mutants demonstrated relatively more stable binding at its stock (highest) concentration with a higher phase shift.

| Mutants | $k_{on}$ | $k_{off}$ | $K_D$ | R Squared | Literature Value |
|---|---|---|---|---|---|
| WT TIL'E' (G99) | 234983 | 0.2875 | 122nM | 0.9551 | 26nM +/- 2nM |
| R816Q | 243936 | 0.1315 | 539nM | 0.9879 | N/A |
| R854Q | 1473202 | 0.2359 | 160nM | 0.9352 | N/A |
| R782W | 284831 | 0.1089 | 380nM | 0.9576 | N/A |
| E787K | 541763 | 0.1295 | 240nM | 0.9891 | N/A |

Table 2. Quantitative data ($k_{on}$ for association, $k_{off}$ for dissociation, and the dissociation constant, $K_D$) for WT TIL'E' as well as each of the mutants.

The G99:ET3i:WT TIL'E' complex bound with a dissociate constant ($K_D$) of 122nM in this study, for comparison and consistency purposes, the TIL'E' mutants will be compared to the obtained WT TIL'E' data at 122nM. It has been noted that the TIL' domain missense causes the most severe form of type 2N vWD, specifically the R816Q mutation. BLI results showed the weakest binding affinity ($K_D$) to FVIII which is consistent with the hypothesis. The loss of the positive charge in the primary negatively charged a3 binding region would cause significant deleterious effects. The significance of R816 electrostatic interaction with FVIII was further confirmed by the cryo-EM structure; BLI data was consistent with the complex structure. E787K and R782W both were hypothesized to affect binding due to potential conformational change of the TIL' domain secondary to changes in charges. BLI data confirmed the decrease in binding to FVIII with 240nM and 380nM, respectively. R782W additionally introduced a more hydrophobic residue, and the increase in hydrophobicity affected its ability to bind to FVIII in comparison to E787K with a 240nM ($K_D$), which is consistent with the hypothesis. Finally, results indicated R854Q had the least amount of effect on binding with the highest binding

affinity out of all the mutants, 160nM. R854Q was hypothesized to only have minimal effect as R854 does not make significant contact with FVIII, and the BLI results were found to be consistent with the cryo-EM structure. All of the mutants, including WT TIL'E', associates quickly on the AMC tip, and dissociates at an incredibly fast rate as well (Figure 31). There were clear phase shifts observed, and a large dissociation phase shift as well (Appendix A Figure 1-5).

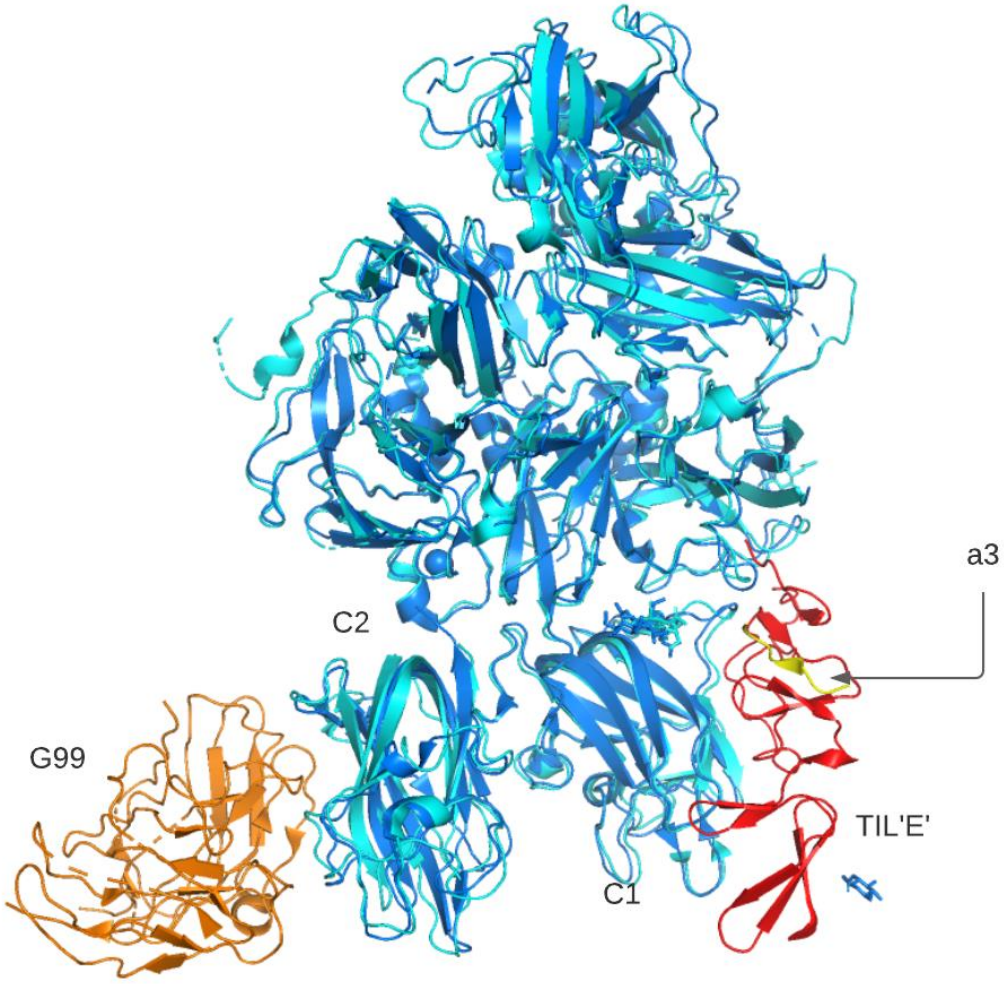


Figure 31. Figure of G99:ET3i complex noted in cyan overlay with the cryo-EM structure of FVIII:vWF complex noted in pale blue. Binding of TIL'E' to the a3 acidic peptide noted in red and yellow, respectively. This is a complex representation utilized in the BLI. Structurally, the G99:ET3i complex binds to the AMC tip, followed by D' of vWF's association. There are no noted binding overlaps, each complex has a different binding motif; with G99 binding at C2, and TIL'E' binding to the a3 and C1 domain of FVIII. (WT TIL'E' PDB ID: 2MHP)

**Affinity Pull-Down Assay**

Qualitative analyses of the TIL'E' mutants against ET3i were conducted via affinity pull down assays with TALON magnetic beads. The TIL'E':ET3i complex served as a control in the affinity pull-down assay. The complex was accomplished by binding TIL'E' to ET3i, to ensure that the tagged proteins and magnetic beads were viable for the assay. The initial TIL'E':ET3i complex was incubated at a 1:1.25 ratio at room temperature prior to the initiation of the assay. Controls showed successful interaction between TIL'E and ET3i, as two bands were visualized in the elution fraction (Figure 24). It was quickly noted that the TIL'E' mutants are not remaining bound to the resin during wash steps. This is evident when comparing the mutants to wild type TIL'E' and D'D3 bound to ET3i (Figure 31). Tagged mutants were bound to the resin, followed by the addition ET3i. Upon wash steps, some protein was lost and subsequently, some of the already limited amounts of ET3i may have also eluted off the column during wash steps. Upon elution, only the bound mutants were visualized on the gel, and no ET3i were detected. Multiple trials have indicated that ET3i has become too dilute to be analyzed on SDS-PAGE. Higher concentrations of ET3i were utilized for this affinity pull-down without significant improvement. The qualitative studies are consistent with the data obtained from the BLI. As quantified, the mutants associate quickly onto the AMC tip with a high $k_{on}$ value, remained bound to ET3i, followed by an incredibly fast off rate ($k_{off}$). This is likely the explanation to the difficulty seen in this binding study.

In figure 32, the most severe type 2N missense (R816Q) along with the mutant that was hypothesized to cause structural perturbation the TIL' domain, R782W, were selected for analysis. In lanes 1-4 are the flow through and wash steps of R816Q:ET3i, and ET3i did indeed

slowly dissociate from R816Q which was bound to the resin. Lane 5 demonstrated an extremely faint line for ET3i (nearly invisible), but R816Q did elute from the column. The lack of ET3i in the complex indicated that ET3i quickly dissociated or was unable to remain bound to R816Q throughout the wash steps. This is consistent with quantitative findings of the weakest dissociation constant ($K_D$) of 539nM when compared to other mutants and wild type (Table 2). Lanes 6 and 7 represent the R782W:ET3i complex, flow through and wash step, respectively. Lane 8 demonstrated the R782W elution fraction, which showed that R782W successfully eluted off the column without the presence of ET3i, as demonstrated by the lack of the ET3i band near 100kDa (Figure 32). The qualitative finding is again consistent with the BLI data of the second weakest binding of 380nM (Table 2). The absence of ET3i on the SDS-PAGE verification has proven to be consistent with the low $K_D$ and quick dissociation rates indicated in the BLI binding kinetics study.

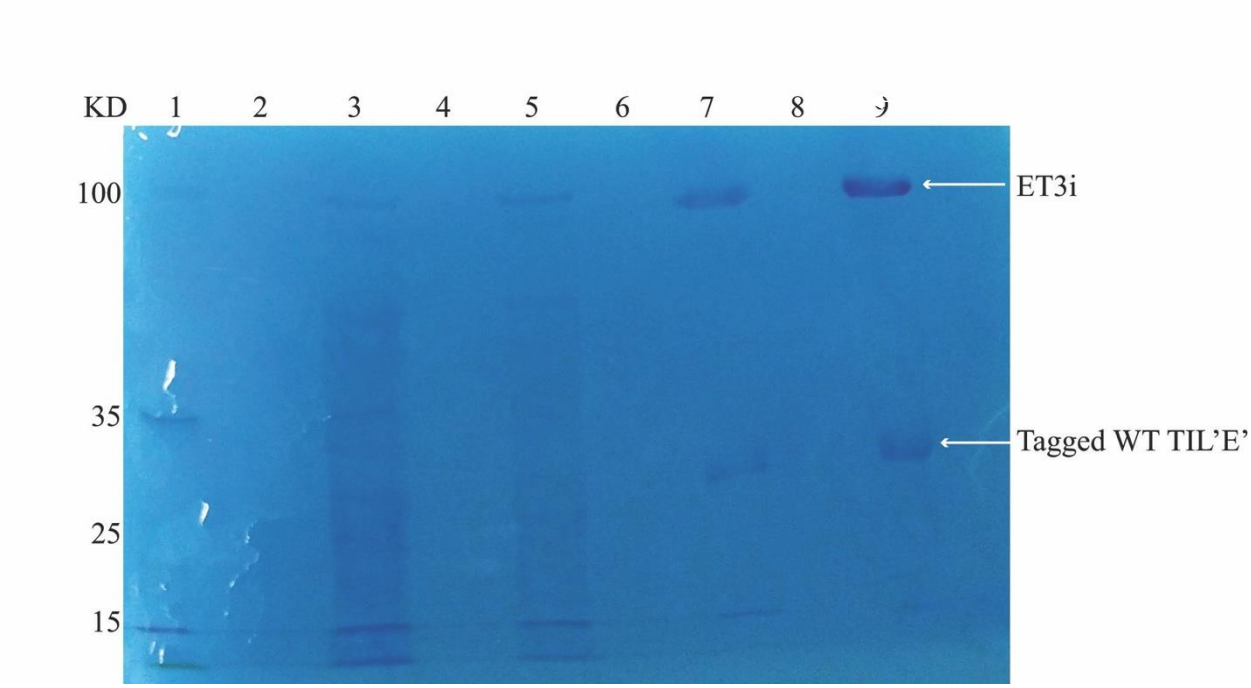


Figure 32. SDS-PAGE verification of protein-protein interaction between WT TIL'E' and ET3i. Lanes: 1. Molecular weight ladder; 2. Intended space; 3. Initial nickel column WT TIL'E' flow through; 4. Intended space; 5. Initial nickel column WT TIL'E' wash fraction; 6. Intended space; 7. WT TIL'E':ET3i wash; 8. intended space; 9. WT TIL'E':ET3i elution fraction.

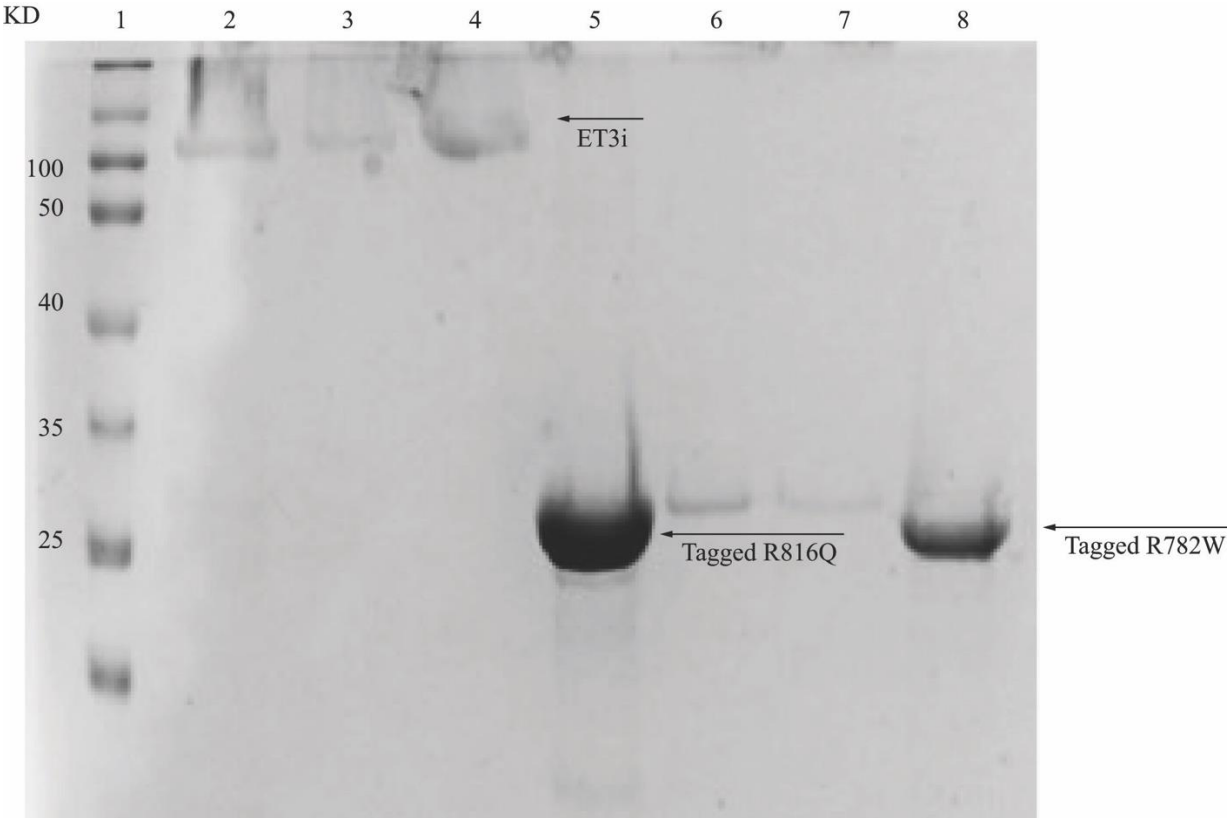


Figure 33. SDS-PAGE verification of R816Q and R782W bound to ET3i. Lanes: 1. Molecular weight protein ladder; 2. R816Q:ET3i flow through; 3. R816:ET3i wash; 4. R816Q:ET3i wash #2; 5. R816Q:ET3i Elution; 6. R782W:ET3i flow through; 7. R782W:ET3i wash; 8. R782W:ET3i elution. SDS-PAGE indicated that tagged TIL'E' and TIL'E' mutants could be visualized but not ET3i upon elution.

**X-Ray Crystallography**

X-ray crystal trials were employed to further study vWF D's structural integrity and its interaction with FVIII. TIL'E':ET3i complexes were complexed for crystallographic trials. Multiple hits were identified from previous lab work sent and done by Hauptman-Woodward Medical Research Institute. The 24-well via hanging drop vapor diffusion crystal trays were set up to further pursue the conditions that contained crystals (Table 3). Initial crystal morphology

was observed to be flat and diamond-like in the wells that contained crystal formation, instead of a traditional three-dimensional crystal morphology. In addition, some of the initial crystals that demonstrated a three-dimensional morphology carried multiple mesh-like layers instead of a thick single-layer appearance. However, there were a few wells that contained full-bodied three-dimensional crystals that were collected for data gathering (Figure 33).

| Screen | Buffer | Salts/(other components) | Precipitants | Manufacturer |
|---|---|---|---|---|
| pH | 0.1M TAPS | Ammonium Sulfate | PEG 12K 12% | Hampton Research |
| | 0.1M TAPS | Ammonium Phosphate | PEG 20K 12% | Hampton Research |
| | 0.1M BTP | Lithium Bromide | PEG 20K 12% | Hampton Research |
| | 0.1M TAPS | Sodium Chloride | PEG 1K 40% | Hampton Research |
| | 0.1M TAPS | Sodium Chloride, Al's Oil | PEG 1K 40% | Hampton Research |
| PEG | 0.1M TAPS (pH 9) | Ammonium Phosphate | PEG 20K | Hampton Research |
| | 0.1M BTP (pH 7.5) | Ammonium Sulfate | PEG 4K | Hampton Research |
| | 0.1M TAPS (pH 9) | Sodium Chloride | PEG 1K | Hampton Research |
| | 0.1M HEPES (pH 7.4) | Sodium Chloride | PEG 4K | Hampton Research |
| | 0.1M BTP (pH 6.5) | Potassium Bromide | PEG 20K | Hampton Research |
| | 0.1M Tris (pH 7.5) | Lithium Bromide | PEG 20K | Hampton Research |

Table 3. crystal trials and well conditions of TIL'E:ET3i complex. The 24 well trays usually consists of two varying components, the x-axis of the tray as well as the Y axis of the tray, while the rest of the components were kept constant (i.e. PEG screen is varying concentrations of PEG on the x-axis, whilst pH screen is varying the pH along the y-axis). All buffers were made from a stock concentration of 1M, salts and other components were diluted from various stock concentrations.

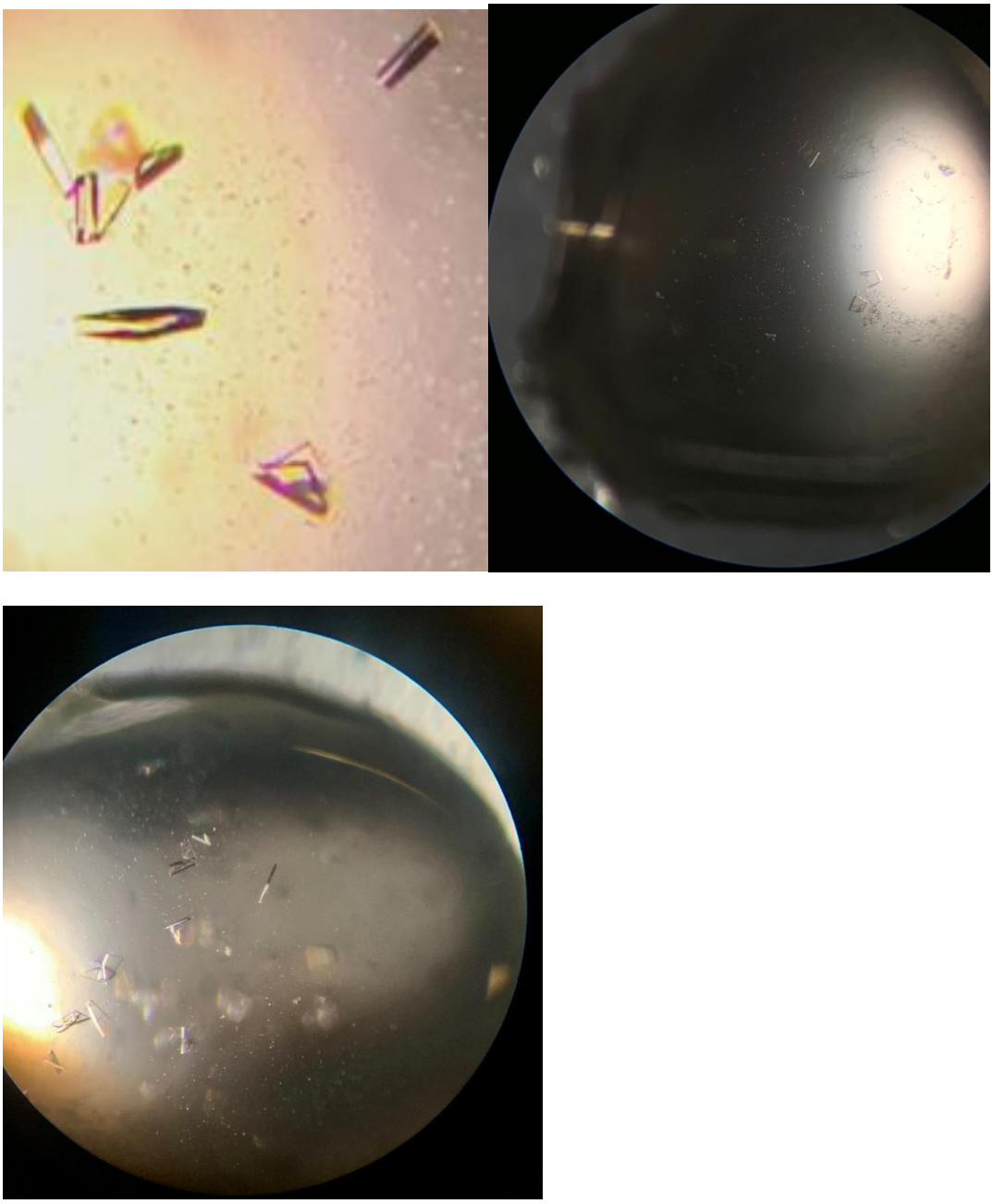

Figure 34. Images of crystals obtained in screens of TIL'E:FVIII complex. Crystal formation observed to be single layered, three dimensional, and diamond-like in appearance.

The crystals in figure 33 were selected, looped, cryo-protected, and screened remotely at THE Advanced Light Source (ALS) at Lawrence Berkeley National Labs, for potential diffraction. The looped crystals were cryoprotected in their growing condition, and promptly

frozen upon extraction. While we were able to grow crystals of ET3i in the presence of vWF D', there was no discernible electron density for TIL'E' in complex with ET3i. However, improved crystallographic conditions were obtained in which there were observed crystal growth, which led to an improved resolution of ET3i.

# Chapter 6

## Conclusion and Future Work

The importance of FVIII's interaction with other proteins and its circulatory partner is demonstrated by the different types of bleeding disorders through its absence or mutations, i.e., hemophilia. Similarly, vWF's interaction with FVIII has been proven to be significant, as mutations may substantially affect their interaction and thus causing von Willebrand Disease. Both hemophilia A and von Willebrand Disease type 2N presents an infinite number of complications, clinical treatments, emergency treatments, and costly financial burdens for its patients. Therefore, structural understanding of FVIII and its circulatory partner, vWF, is crucial to further understand the formation of these bleeding disorder. Improved understanding of these two large glycoproteins is necessary to improve and enhance therapeutic treatments and patient care.

New publications in the recent years have made significant strides towards structural knowledge between FVIII, isolated domains of FVIII, vWF, D', and D'D3 domains of FVIII. A negative-stain electron microscopy and hydrogen-deuterium mass spectroscopy (HDX-MS) studies with D'D3 was previously conducted.[53] The findings Chiu et al. substantiate those of Yee et al. where C1 was established as the major vWF binding site.[57,58] With the most recent publication of the high-resolution structure paved way for a better understanding for hemophilia A as well as von Willebrand Diseases. This 2.9Å structure determined the binding mechanism of how FVIII's circulatory partner, vWF, interacts with it. As discussed earlier, vWF D' domain has been proposed to be the domain that is highly involved in the binding to FVIII. Fuller et al. were able to confirm this interaction from their complex structure.[47] Furthermore, severe hemophilia A

and type 2N von Willebrand disease mutants were identified and discussed structurally. Fuller et al. confirmed the significant electrostatic interaction between R816 and sulfated Y1680 in the C1 domain of FVIII (Figure 34).[55]

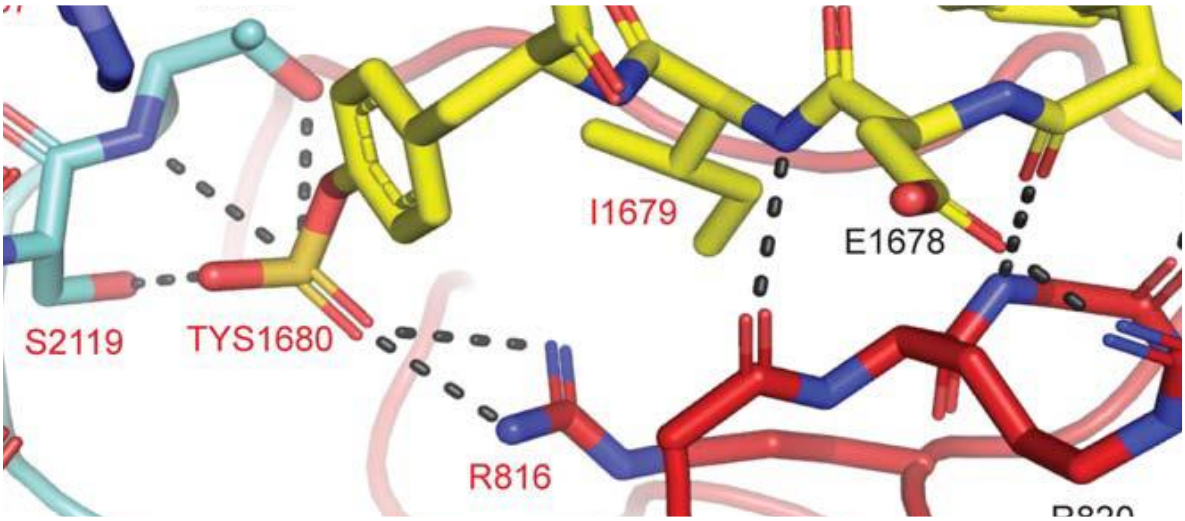


Figure 35. sulfated Tyr1680 interacting with the TIL' domain R816 residue. The electrostatic interactions are noted in gray dotted lines and constitutes as stabilizing force for FVIII and vWF.

Contradictory to recent publication of interaction of vWF and C2 domain, the cryo-EM structure indicated that D' does not involve the C2 domain when docked onto FVIII. Instead, D' makes the most significant amount of contact with the a3 and C1 domain of FVIII, and the D3 domain of vWF contacts C2 domain of FVIII (Figure 27).[52] The binding studies conducted in the Spiegel Lab were evaluated and consistent with the most recent structure. The rapid association and dissociation of all TIL'E' mutants indicated certain deleterious effects. Quantitatively, changes in binding that are measured 10-fold or greater usually indicates a confirmed binding disturbance. However, the mutants' disruption in binding to FVIII were only measured to be five-fold less than wild type TIL'E' (Table 2). Thus, it may be concluded that even a small structural change or a change in electrostatic charges (structural perturbation) is significant

enough to affect vWF's ability to bind to FVIII. In other words, the stability of FVIII:vWF binding may be easily disturbed, as evaluated through the BLI. Though the TIL'E'-Mutants:FVIII complexes were unseen in structure (via crystallography), the binding capabilities were quantitatively evaluated via BLI. The instabilities in binding observed in the studies that were conducted in the research lab allowed further hypotheses and trajectories of research.

All cumulative efforts on the structure of FVIII allowed Fuller's group to uncover the most recent high-resolution structure. The cryo-EM structure verified that neither the C1 domain alone nor the acidic peptide region (a3) alone were sufficient to establish stable complexes with the vWF domains. The newly published FVIII:D'D3 structure created exciting opportunities for the future of the blood community, as it serves as a foundation for all other FVIII or vWF mutant studies that cause other types of bleeding disorders. Researchers have often overlooked FVIII's interactions with other proteins in circulation, this new structural finding may serve a great purpose in understanding other intricacies of FVIII in circulation. With better understanding of FVIII and its other protein interactions, improved therapeutic strategies can subsequently be made for patients who are suffering from FVIII or von Willebrand related disorders.

References


1. Kingdon, H. S., Davie, E. W. & Ratnoff, O. D. The Reaction between Activated Plasma Thromboplastin Antecedent and Diisopropylphosphofluoridate. *Biochemistry* (1964) doi:10.1021/bi00890a005.
2. Davie, E. W., Fujikawa, K. & Kisiel, W. The Coagulation Cascade: Initiation, Maintenance, and Regulation. *Biochemistry* (1991) doi:10.1021/bi00107a001.
3. Hoffman, M., Monroe, D. M. & Roberts, H. R. Cellular interactions in hemostasis. *Pathophysiol. Haemost. Thromb.* (1996) doi:10.1159/000217233.
4. Webster, W. P. *et al.* Factor VIII synthesis: hepatic and renal allografts in swine with von Willebrand's disease. *Am. J. Physiol.* (1976) doi:10.1152/ajplegacy.1976.230.5.1342.
5. Eaton, D., Rodriguez, H. & Vehar, G. A. Proteolytic Processing of Human Factor VIII. Correlation of Specific Cleavages by Thrombin, Factor Xa, and Activated Protein C with Activation And Inactivation of Factor VIII Coagulant Activity. *Biochemistry* (1986) doi:10.1021/bi00350a035.
6. Vehar, G. A. *et al.* Structure of human factor VIII. *Nature* (1984) doi:10.1038/312337a0.
7. Foster, P. A., Fulcher, C. A., Marti, T., Titani, K. & Zimmerman, T. S. A major factor VIII binding domain resides within the amino-terminal 272 amino acid residues of von Willebrand factor. *J. Biol. Chem.* **262**, 8443–8450 (1987).
8. Hill-Eubanks, D. C., Parker, C. G. & Lollar, P. Differential proteolytic activation of factor VIII-von Willebrand factor complex by thrombin. *Proc. Natl. Acad. Sci. U. S. A.* (1989) doi:10.1073/pnas.86.17.6508.
9. Saenko, E. L. & Scandella, D. The acidic region of the factor VIII light chain and the C2

domain together form the high affinity binding site for von Willebrand factor. *J. Biol. Chem.* **272**, 18007–18014 (1997).

10. Lollar, P. & Parker, C. G. Subunit Structure of Thrombin-Activated Porcine Factor VIII. *Biochemistry* (1989) doi:10.1021/bi00428a038.

11. Smith, I. W. *et al.* The 3.2 Å structure of a bioengineered variant of blood coagulation factor VIII indicates two conformations of the C2 domain. *J. Thromb. Haemost.* (2020) doi:10.1111/jth.14621.

12. Soucie, J. M., Evatt, B. & Jackson, D. Occurrence of hemophilia in the United States. *Am. J. Hematol.* (1998) doi:10.1002/(SICI)1096-8652(199812)59:4<288::AID-AJH4>3.0.CO;2-I.

13. White, G. *et al.* Definitions in Hemophilia. *Thromb. Haemost.* (2001) doi:10.1055/s-0037-1615621.

14. Gitschier, J. *et al.* Characterization of the human factor VIII gene. *Nature* (1984) doi:10.1038/312326a0.

15. Coppola, A., Santoro, C., Tagliaferri, A., Franchini, M. & Di Minno, G. Understanding inhibitor development in haemophilia A: Towards clinical prediction and prevention strategies. *Haemophilia* **16**, 13–19 (2010).

16. Addiego, J. E. *et al.* Treatment of hemophilia a with a highly purified factor VIII concentrate prepared by Anti-FVIIIc immunoaffinity chromatography. *Thromb. Haemost.* **67**, 19–27 (1992).

17. Treatment of Hemophilia | CDC. https://www.cdc.gov/ncbddd/hemophilia/treatment.html.

18. O, A. *et al.* Baby hamster kidney cell-derived recombinant factor VIII: a quarter century of learning and clinical experience. *Expert Rev. Hematol.* **9**, 1151–1164 (2016).

19. Konkle, B. A. *et al.* Pegylated, full-length, recombinant factor VIII for prophylactic and on-demand treatment of severe hemophilia A. *Blood* **126**, 1078–1085 (2015).

20. Pfristershammer, K. *et al.* Recombinant factor VII and factor VIII-von Willebrand factor complex do not present danger signals for human dendritic cells. *Thromb. Haemost.* **96**, 309–316 (2006).

21. Hoffman, M. & Dargaud, Y. Mechanisms and monitoring of bypassing agent therapy. *Journal of Thrombosis and Haemostasis* (2012) doi:10.1111/j.1538-7836.2012.04793.x.

22. Zhou, Y. F. *et al.* Sequence and structure relationships within von Willebrand factor. *Blood* **120**, 449–458 (2012).

23. Dumont, J. A. *et al.* Prolonged activity of a recombinant factor VIII-Fc fusion protein in hemophiliaA mice and dogs. *Blood* **119**, 3024–3030 (2012).

24. K, K.-T. *et al.* Recombinant factor VIII Fc fusion protein drives regulatory macrophage polarization. *Blood Adv.* **2**, 2904–2916 (2018).

25. Horling, F. M. *et al.* Immunogenicity of BAX 855 in Previously Treated Patients with Congenital Severe Hemophilia A. *Blood* (2016) doi:10.1182/blood.v128.22.2594.2594.

26. Kitazawa, T. & Shima, M. Emicizumab, a humanized bispecific antibody to coagulation factors IXa and X with a factor VIIIa-cofactor activity. *Int. J. Hematol.* (2020) doi:10.1007/s12185-018-2545-9.

27. Sampei, Z. *et al.* Identification and Multidimensional Optimization of an Asymmetric Bispecific IgG Antibody Mimicking the Function of Factor VIII Cofactor Activity. *PLoS One* (2013) doi:10.1371/journal.pone.0057479.

28. Shima, M. *et al.* Factor VIII–Mimetic Function of Humanized Bispecific Antibody in Hemophilia A. *https://doi.org/10.1056/NEJMoa1511769* **374**, 2044–2053 (2016).

29. Prescott, R. *et al.* The inhibitor antibody response is more complex in hemophilia a patients than in most nonhemophiliacs with factor VIII autoantibodies. *Blood* (1997) doi:10.1182/blood.v89.10.3663.

30. Brison, C. M. *et al.* The 1.7 Å X-ray crystal structure of the porcine factor VIII C2 domain and binding analysis to anti-human C2 domain antibodies and phospholipid surfaces. *PLoS One* (2015) doi:10.1371/journal.pone.0122447.

31. Walter, J. D. *et al.* Thrombosis and hemostasis: Structure of the factor VIII C2 domain in a ternary complex with 2 inhibitor antibodies reveals classical and nonclassical epitopes. *Blood* (2013) doi:10.1182/blood-2013-08-519124.

32. Ronayne, E. K. *et al.* Structure of Blood Coagulation Factor VIII in Complex With an Anti-C2 Domain Non-Classical, Pathogenic Antibody Inhibitor. *Front. Immunol.* (2021) doi:10.3389/fimmu.2021.697602.

33. BERNTORP, P. D. E. *et al.* von Willebrand's disease: a report from a meeting in the Åland islands. *Haemophilia* **18**, 1 (2012).

34. Larrieu, M. J. *et al.* Congenital bleeding disorders with long bleeding time and normal platelet count. II. Von Willebrand's disease (report of thirty-seven patients). *Am. J. Med.* (1968) doi:10.1016/0002-9343(68)90070-3.

35. Ewenstein, B. M. Von Willebrand's disease. *Annual Review of Medicine* (1997) doi:10.1146/annurev.med.48.1.525.

36. Donnér, M. *et al.* Type IIB von Willebrand's disease: gene mutations and clinical presentation in nine families from Denmark, Germany and Sweden. *Br. J. Haematol.* (1992) doi:10.1111/j.1365-2141.1992.tb04594.x.

37. Nishino, M., Girma, J. P., Rothschild, C., Fressinaud, E. & Meyer, D. New variant of von

Willebrand disease with defective binding to factor VIII. *Blood* (1989) doi:10.1182/blood.v74.5.1591.bloodjournal7451591.

38. Rodeghiero, F., Castaman, G. & Dini, E. Epidemiological investigations of the prevalence of von Willebrand's disease. *Blood* (1987) doi:10.1182/blood.v69.2.454.bloodjournal692454.

39. Mannucci, P. M., Pareti, F. I., Ruggeri, Z. M. & Capitanio, A. 1-DEAMINO-8-D-ARGININE VASOPRESSIN: A NEW PHARMACOLOGICAL APPROACH TO THE MANAGEMENT OF HAEMOPHILIA AND VON WILLEBRAND'S DISEASE. *Lancet* (1977) doi:10.1016/S0140-6736(77)91197-7.

40. Sadler, J. E. Von Willebrand disease type 1: A diagnosis in search of a disease. *Blood* (2003) doi:10.1182/blood-2002-09-2892.

41. Eikenboom, J. C. J. Congenital von Willebrand disease type 3: Clinical manifestations, pathophysiology and molecular biology. *Best Pract. Res. Clin. Haematol.* (2001) doi:10.1053/beha.2001.0139.

42. Sadler, J. E. *et al.* Update on the pathophysiology and classification of von Willebrand disease: A report of the Subcommittee on von Willebrand factor. *J. Thromb. Haemost.* (2006) doi:10.1111/j.1538-7836.2006.02146.x.

43. Allen, S. *et al.* Two novel type 2N von Willebrand disease-causing mutations that result in defective factor VIII binding, multimerization, and secretion of von Willebrand factor. *Blood* (2000) doi:10.1182/blood.v95.6.2000.

44. Blenner, M. A., Dong, X. & Springer, T. A. Structural basis of regulation of von Willebrand factor binding to glycoprotein Ib. *J. Biol. Chem.* (2014) doi:10.1074/jbc.M113.511220.

45. Koedam, J. A., Meijers, J. C. M., Sixma, J. J. & Bouma, B. N. Inactivation of human Factor VIII by activated protein C. Cofactor activity of protein S and protective effect of von Willebrand factor. *J. Clin. Invest.* (1988) doi:10.1172/JCI113721.

46. Nesheim, M. *et al.* The effect of plasma von Willebrand factor on the binding of human factor VIII to thrombin-activated human platelets. *J. Biol. Chem.* (1991) doi:10.1016/s0021-9258(18)55200-5.

47. Verweij, C. L., Diergaarde, P. J., Hart, M. & Pannekoek, H. Full-length von Willebrand factor (vWF) cDNA encodes a highly repetitive protein considerably larger than the mature vWF subunit. *EMBO J.* (1986) doi:10.1002/j.1460-2075.1986.tb04435.x.

48. Titani, K. *et al.* Amino Acid Sequence of Human von Willebrand Factor. *Biochemistry* (1986) doi:10.1021/bi00359a015.

49. Bonthron, D. T. *et al.* Structure of pre-pro-von willebrand factor and its expression in heterologous cells. *Nature* (1986) doi:10.1038/324270a0.

50. Bonthron, D. *et al.* Nucleotide sequence of pre-pro-von willebrand factor cDNA. *Nucleic Acids Res.* (1986) doi:10.1093/nar/14.17.7125.

51. Shelton-Inloes, B. B., Broze, G. J., Miletich, J. P. & Sadler, J. E. Evolution of human von Willebrand factor: CDNA sequence polymorphisms, repeated domains, and relationship to von Willebrand antigen II. *Biochem. Biophys. Res. Commun.* (1987) doi:10.1016/S0006-291X(87)80016-5.

52. Nachman, R., Levine, R. & Jaffe, E. A. Synthesis of factor VIII antigen by cultured guinea pig megakaryocytes. *J. Clin. Invest.* (1977) doi:10.1172/JCI108846.

53. Zhou, Y. F. *et al.* Sequence and structure relationships within von Willebrand factor. *Blood* **120**, 449–458 (2012).

54. Dagil, L. *et al.* Interaction Between the a3 Region of Factor VIII and the TIL'E' Domains of the von Willebrand Factor. *Biophys. J.* (2019) doi:10.1016/j.bpj.2019.07.007.

55. Fuller, J. R., Knockenhauer, K. E., Leksa, N. C., Peters, R. T. & Batchelor, J. D. Molecular determinants of the factor VIII/von Willebrand factor complex revealed by BIVV001 cryo-electron microscopy. *Blood* (2021) doi:10.1182/blood.2020009197.

56. Shiltagh, N. *et al.* Solution structure of the major factor VIII binding region on von Willebrand factor. *Blood* **123**, 4143–4151 (2014).

57. Chiu, P. L. *et al.* Mapping the interaction between factor VIII and von Willebrand factor by electron microscopy and mass spectrometry. *Blood* (2015) doi:10.1182/blood-2015-04-641688.

58. Yee, A. *et al.* Visualization of an N-terminal fragment of von Willebrand factor in complex with factor VIII. *Blood* (2015) doi:10.1182/blood-2015-04-641696.

59. Scandella, D. *et al.* Some factor VIII inhibitor antibodies recognize a common epitope corresponding to C2 domain amino acids 2248 through 2312, which overlap a phospholipid-binding site. *Blood* (1995) doi:10.1182/blood.v86.5.1811.bloodjournal8651811.

60. Saenko, E. L., Shima, M., Rajalakshmi, K. J. & Scandella, D. A role for the C2 domain of factor VIII in binding to von Willebrand factor. *J. Biol. Chem.* (1994) doi:10.1016/s0021-9258(19)78167-8.

## Appendix A

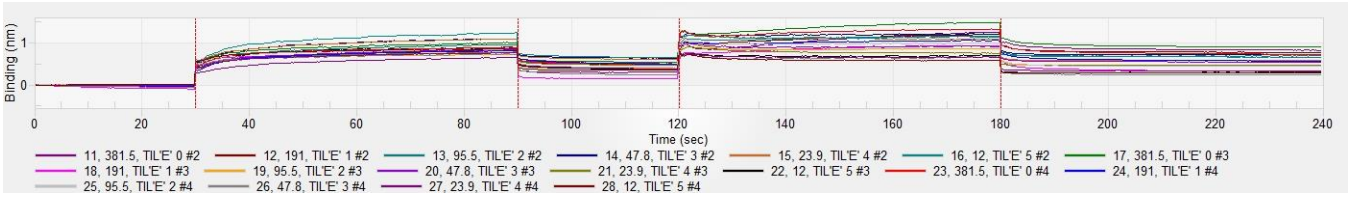


Figure 1. Biolayer interferometry (BLI) binding signal representation (in triplicate) of G99:ET3i complex against wild tyle TIL'E'. It was observed that wild type TIL'E' did not associate well to the AMC tip with a quick observable association and dissociation rate.

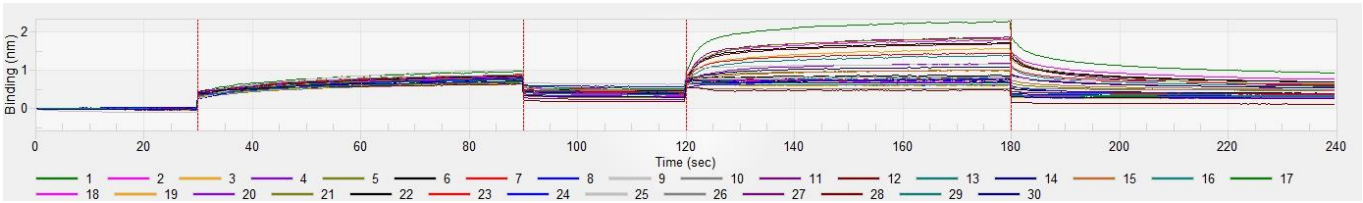


Figure 2. Biolayer interferometry (BLI) binding signal representation (in triplicate) of G99:ET3i complex against R816Q. It was observed that there was a strong phase shift at stock R854Q (highest) concentration in comparison to wild type. This association rate was observed in quantitative data analysis.

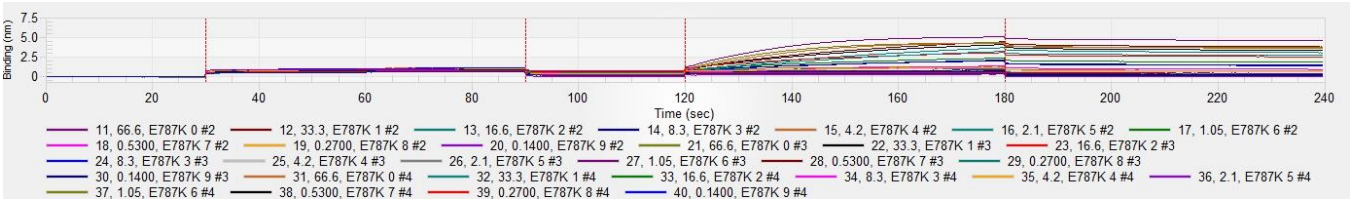


Figure 3. Biolayer interferometry (BLI) binding signal representation (in triplicate) of G99:ET3i complex against E787K mutant. Steady decrease in binding with decreasing concentrations of mutant.

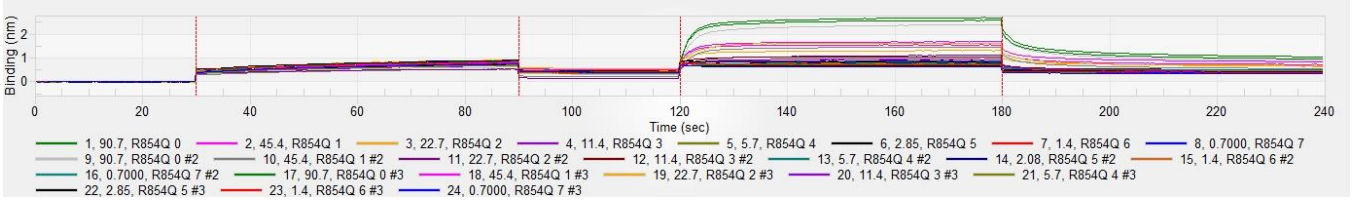

Figure 4. Biolayer interferometry (BLI) binding signal representation (in triplicate) of G99:ET3i complex against R854Q mutant. Similar visual representation compared to R816Q mutant.

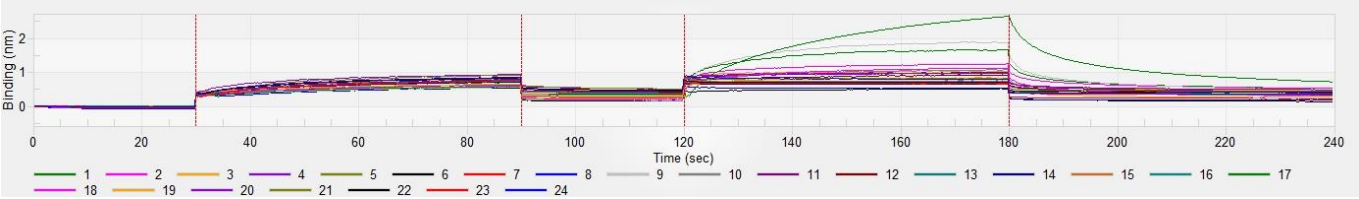


Figure 5. Biolayer interferometry (BLI) binding signal representation (in triplicate) of G99:ET3i complex against R782W mutant. It was observed that there was a strong phase shift at stock R782W (highest) concentration like all TIL'E' mutants with a quick change in poor signaling upon lower concentrations of R782W.